NASA Technical Memorandum 80077

RECENT DEVELOPMENTS IN THE DESIGN, TESTING AND IMPACT-DAMAGE TOLERANCE OF STIFFENED COMPOSITE PANELS

Jerry G. Williams; Melvin S. Anderson;
Marvin D. Rhodes; James H. Starnes, Jr.; and
W. Jefferson Stroud

April 1979

(NASA-TM-80077) RECENT DEVELOPMENT IN THE DESIGN, TESTING AND IMPACT-DAMAGE TOLERANCE OF STIFFENED COMPOSITE PANELS (NASA) 34 p HC A03/MF A01 CSCL 20K
N79-22566
Unclas
G3/39 25137

RECEIVED
NASA STI FACILITY
ACCESS DEPT.
1979

National Aeronautics and
Space Administration

Langley Research Center
Hampton, Virginia 23665

RECENT DEVELOPMENTS IN THE DESIGN, TESTING AND IMPACT-DAMAGE TOLERANCE OF STIFFENED COMPOSITE PANELS

Jerry G. Williams; Melvin S. Anderson; Marvin D. Rhodes;
James H. Starnes, Jr.; and W. Jefferson Stroud

National Aeronautics and Space Administration
Langley Research Center
Hampton, Virginia

SUMMARY

Structural technology of laminated filamentary-composite stiffened-panel structures under combined inplane and lateral loadings is discussed. Attention is focused on (1) methods for analyzing the behavior of these structures under load and for determining appropriate structural proportions for weight-efficient configurations, and (2) effects of impact damage and geometric imperfections on structural performance. Recent improvements in buckling analysis involving combined inplane compression and shear loadings and transverse shear deformations are presented. A computer code is described for proportioning or sizing laminate layers and cross-sectional dimensions, and the code is used to develop structural efficiency data for a variety of configurations, loading conditions, and constraint conditions. Experimental data on buckling of panels under inplane compression is presented to validate the analysis and sizing methods and to illustrate structural performance and efficiency obtained from representative structures. Experimental results show that strength of panels under inplane compression can be degraded by low-velocity impact damage. Mechanisms of impact-damage initiation and propagation are described. Finally, data are presented that indicates the matrix is a significant factor influencing tolerance to impact damage.

INTRODUCTION

To take advantage of the mass-saving potential of advanced composite materials, procedures must be developed that provide reliable and efficient structural designs. In addition to satisfying traditional design requirements typical of metal structures, composite structural designs must also account for characteristics and failure modes unique to composite materials. Once these features are understood, analytical methods can be developed to predict the behavior of structural components made of composites, and appropriate criteria can be imposed to insure that efficient composite structures meet all design requirements.

One research focus at the NASA Langley Research Center has been the development of analysis and sizing methods for composite structural panels required to carry compression and combined loads. A state-of-the-art review of these studies was presented in 1975 which included an investigation of panel buckling as well as the effects of low-velocity impact damage on composite sandwich panels (ref. 1). During the past three years, considerable progress has been made in understanding the structural behavior of stiffened composite panels and several failure mechanisms that affect the performance of compression panels subjected to low-velocity impact damage have been identified. The graphite-epoxy

ORIGINAL PAGE IS
OF POOR QUALITY

materials from which the panels were fabricated are commercially available 450K cure temperature systems which were processed in an autoclave following the manufacturer's recommended procedures. The present paper summarizes Langley research activities conducted since 1975 on stiffened composite panels. Advances in analysis and sizing procedures for stiffened compression panels are discussed, and experiments conducted to verify these analysis and sizing procedures are described. The effect of low-velocity impact damage on the strength of compression panels is also presented.

SYMBOLS

A	Planform area of stiffened panel.
B	Width.
E_{11}	Young's modulus of composite material in fiber direction.
ET	Longitudinal extensional stiffness of panel.
e	Amplitude of overall bow at panel midlength.
G_{44}	Transverse shear modulus.
GT	Shear stiffness of panel.
L	Panel length.
N_x, N_y, N_{xy}	Stress resultants.
N_x/L	Load index.
P	Lateral pressure loading on panel.
t	Thickness.
W	Mass of stiffened panel.
$\frac{W/A}{L}$	Mass index.
Δ	Amplitude of eccentricity at panel midwidth.
ε	Strain at buckling.

STIFFENED PANEL ANALYSIS AND SIZING

The complexities of laminated composite panels have led to development of sophisticated analysis and design procedures compared to those formerly used for metal panels. Panels must be designed to carry combined loads and structural efficiency and manufacturing considerations require that a variety of structural configurations be considered (see figure 1). The VIPASA computer code (ref. 2) is an example of a sophisticated analysis program for the rapid and accurate buckling solution of stiffened composite panels subjected to compression loading. VIPASA, however, gives conservative solutions for the general buckling mode of a rectangular panel subjected to shear loading and does not include the effects of through-the-thickness transverse shear deformations. Approaches for improving the solution for both of these problems, and typical examples are described herein. In addition, a sizing code called PASCO (Panel Analysis and Sizing Code) which uses VIPASA to perform buckling analyses is described, and the PASCO code is used to provide structural efficiency results for important generic classes of problems.

ORIGINAL PAGE IS
OF POOR QUALITY

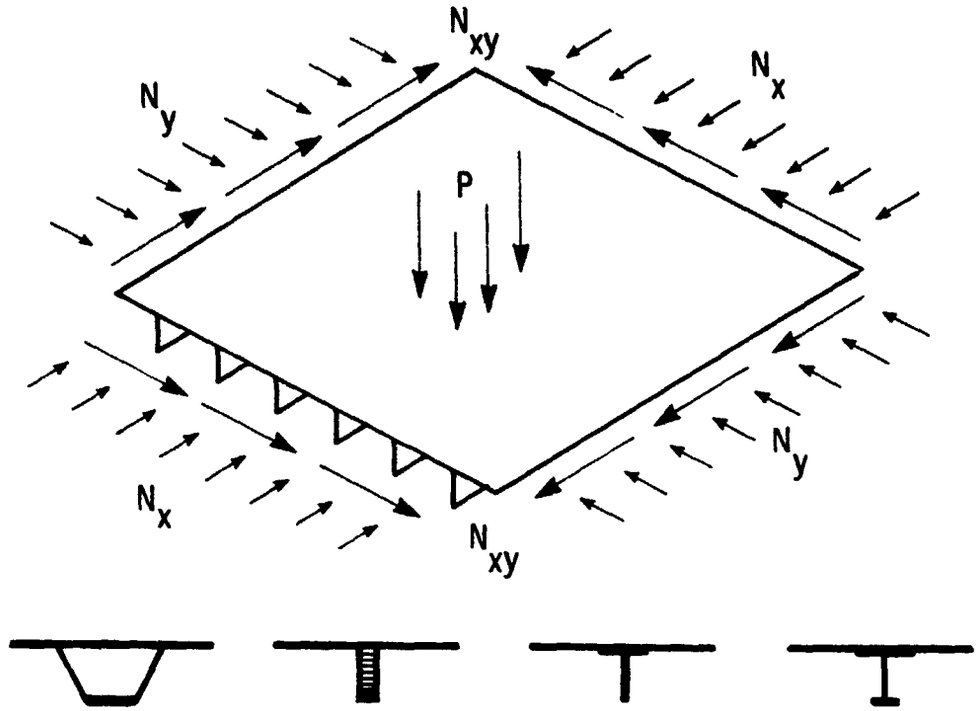

Figure 1.- Stiffened panel subjected to combined loads and representative stiffener configurations.

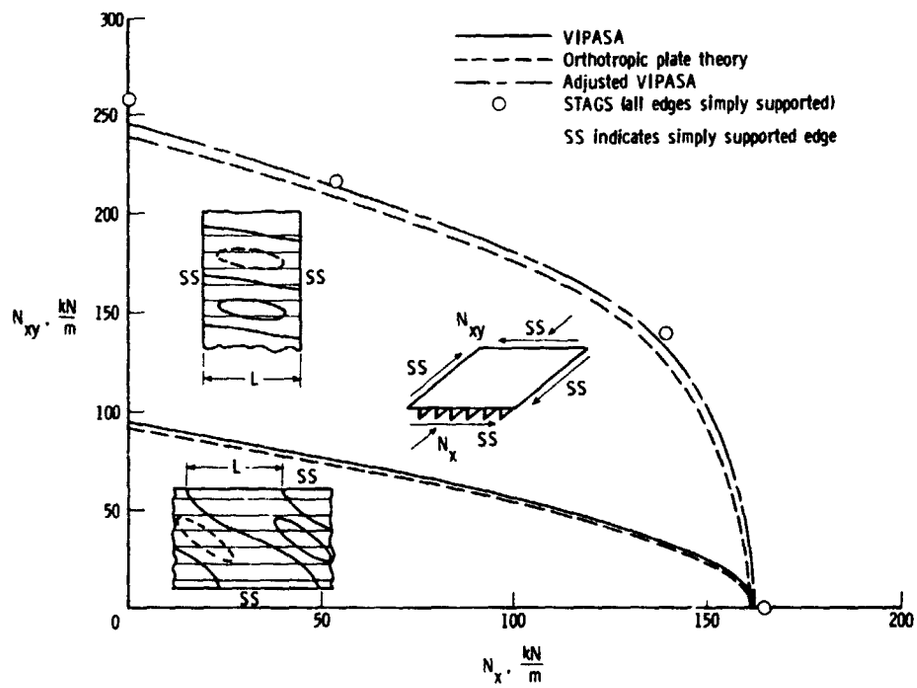

Figure 2.- Comparison of predicted buckling loads from various analyses for blade-stiffened panel subjected to combined longitudinal compression and shear loadings.

Stiffened Panel Stability Analysis

Combined shear and compression loads.- The VIPASA buckling analysis (ref. 2) provides an exact solution to the classical thin-plate equations which are based on the Kirchhoff-Love hypothesis. The buckling solution is obtained by assuming a sinusoidal buckle pattern in the stiffener direction. A sinusoidal buckle pattern assumption for orthotropic panels loaded by inplane longitudinal and transverse loads permits simple support boundary conditions to be satisfied on edges normal to the stiffeners while the boundary condition on edges parallel to the stiffeners may be arbitrarily specified. The presence of shear or anisotropy causes skewed node lines which do not conform to the panel rectangular boundaries. In these situations, the resulting theoretical solutions are lower than that given by the solution from a two-dimensional analysis in which the desired boundary conditions are accurately modeled. The error introduced by anisotropy for most practical configurations is small, but the buckling strain for the general mode ($m = 1$) of a panel loaded in shear can be substantially in error. Buckling solutions for local modes in which more than one buckle forms along the length, however, are accurately predicted by VIPASA.

Because of the complexity and computer expense of a full two-dimensional analysis, an approximate method based on a combination of VIPASA and orthotropic plate theory has been developed for panels subjected to combined shear and compression loading. Typical interaction curves for shear and compression are shown in figure 2 for a 76.2-cm-square, blade-stiffened composite panel having six stiffeners. Materials properties used in the analysis are presented in Table I (material A-tape) and cross sectional dimensions are defined in Table II (design B). The desired boundary conditions are simple support on all four edges. In the VIPASA analysis, however, boundary conditions can be specified only on the two edges parallel to the stiffeners. The results of this analysis are presented as the solid curve in figure 2. VIPASA was also used to obtain the buckling load of the panel simply supported along the side edges assuming smeared orthotropic stiffness properties (lower dash curve). Differences in these two results are attributed to the inadequacy of representing the stiffened panel by average orthotropic stiffnesses. The same orthotropic panel can be analyzed by VIPASA with the edges perpendicular to the stiffeners simply supported. This result (the upper dashed curve) shows a large increase in buckling load reflecting the fact that it is more important to model correctly the boundary conditions on the edge normal to the stiffening. It is postulated that any difference in the lower two curves would be similar to the difference between the upper curve for the VIPASA analyses using orthotropic stiffnesses and an exact analysis of the detailed cross section with ends simply supported. Thus, the ratio of the two lower results is applied to the upper curve to give the curve labeled Adjusted VIPASA.

The accuracy of the approach for predicting the buckling of rectangular panels loaded in shear is indicated by a few results obtained from the STAGS computer program (ref. 3) which treated the detailed panel simply supported on all four edges. Either of the two upper curves provide a conservative but reasonably accurate estimate of the correct result obtained from the two dimensional STAGS analysis. Not satisfying boundary conditions on the side edges of stiffened panels leads to little error because the node lines tend to align approximately with the stiffeners and several buckles form across the width. For certain configurations where local stiffener deformation is pronounced, the adjusted VIPASA result can be significantly lower than the orthotropic plate results with simply supported edges. The conservative approach of choosing the lower of these two approximate solutions is used herein. Additional studies have been made with the approximate analysis that show it to be in reasonable agreement with more accurate analyses whenever the buckle length transverse to the stiffeners is greater than twice the stiffener spacing. In the example shown in figure 2, the buckle length transverse to the stiffeners was approximately 3 stiffener spacings. Design studies on panels loaded by shear and biaxial compression have shown that using the conservative VIPASA solution leads to only a few percent mass penalty for most practical load combinations. If shear is the dominant loading, the approximate analysis can be used to take advantage of the greater predicted load carrying capability if proper caution is used in evaluating the results based on the calculated buckling mode shapes. The advantages of the approximate analysis relative to a two-

ORIGINAL PAGE IS
OF POOR QUALITY

TABLE I.- GRAPHITE-EPOXY LAMINA PROPERTIES

	MATERIAL A		MATERIAL B
	Tape	Fabric	Tape
Modulus in fiber direction, GPa	131.0	62.7	110.0
Modulus normal to fibers, GPa	13.0	62.7	-
Shear modulus, GPa	6.4	6.4	-
Major Poisson's ratio	0.38	0.10	-
Density, Mg/m^3	1.52	1.52	1.60
Thickness, mm/ply	0.14	0.36	.17

dimensional analysis are (1) less effort is required in data preparation, (2) a solution convergence check is not required and (3) three orders of magnitude less computer time is required.

Transverse shear effects.- Composite panels with open-section stiffeners such as blade stiffeners have been shown (ref. 4) to require a higher mass to carry a specified compression load than stiffened panels with closed-section stiffeners such as hat stiffeners. One open-section stiffener configuration which has been shown to have improved structural efficiency is the sandwich-blade (ref. 5) in which the web is of sandwich construction and connects the panel skin to a cap composed mostly of 0° oriented plies. However, some of the advantage of this configuration is offset by the low transverse shear stiffness of the honeycomb core.

The VIPASA analysis does not include transverse shear deformations, although finite element codes such as NASTRAN (ref. 6) have plate elements which do include transverse shear deformations in the buckling formulation. However, an analysis more rapid than NASTRAN is desired that can be incorporated in a structural sizing code. One such analysis has been developed and is presented in reference 5.

An illustration taken from reference 5 showing the influence of transverse shear on buckling is presented in figure 3. The buckling strain is presented as a function of the buckle length for designs having a honeycomb core with transverse shear modulus values of 0.26 GPa, 1.21 GPa, and for an infinite transverse shear modulus. The solution with infinite transverse shear modulus was obtained using the BUCLASP2 computer code (ref. 7). The dimensions of the cross section and the number of plies in each element are presented in Table II as design A. For the results shown in figure 3, three buckling modes occur including local buckling of the skin, twisting of the stiffener, and wide-column buckling of the panel. In the range of buckle length for which twisting is the buckling mode (10 to 70 cm), the buckling strain is strongly dependent on the transverse shear stiffness of the core. For a 30-cm-long buckle length, for example, the 0.26 GPa shear modulus reduces the buckling strain by 40 percent relative to the solution for infinite shear

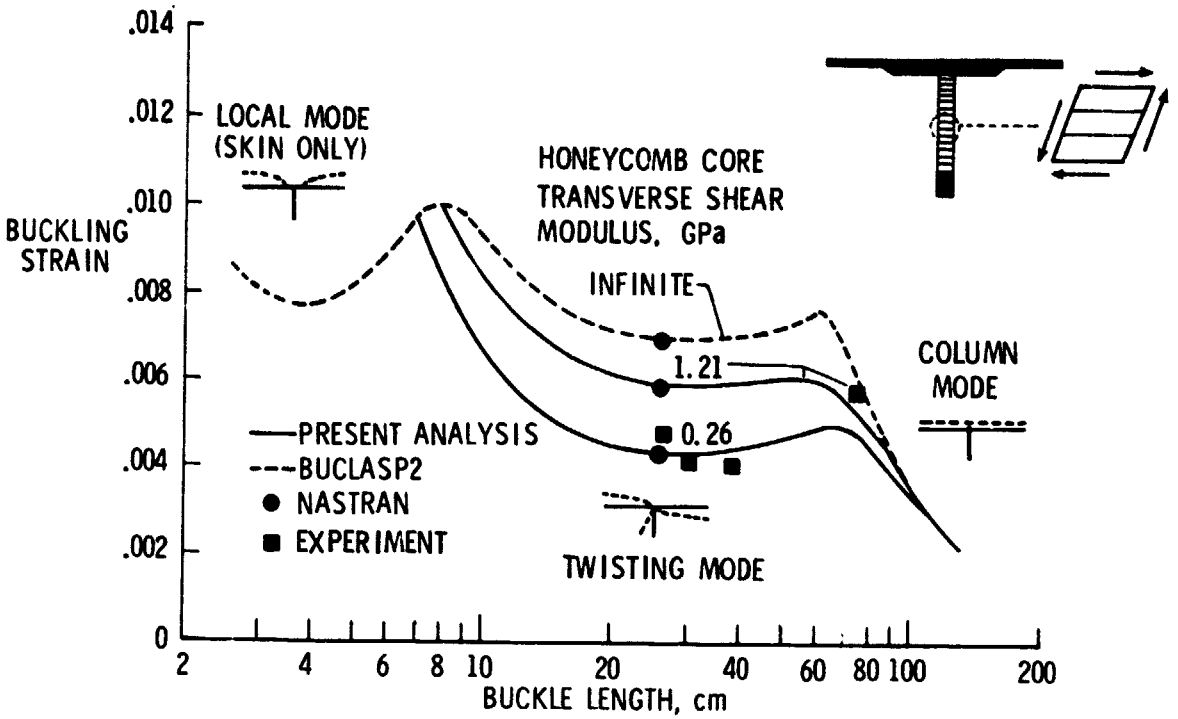

Figure 3.- Effect of transverse shear on the buckling strain of a sandwich-blade stiffened panel.

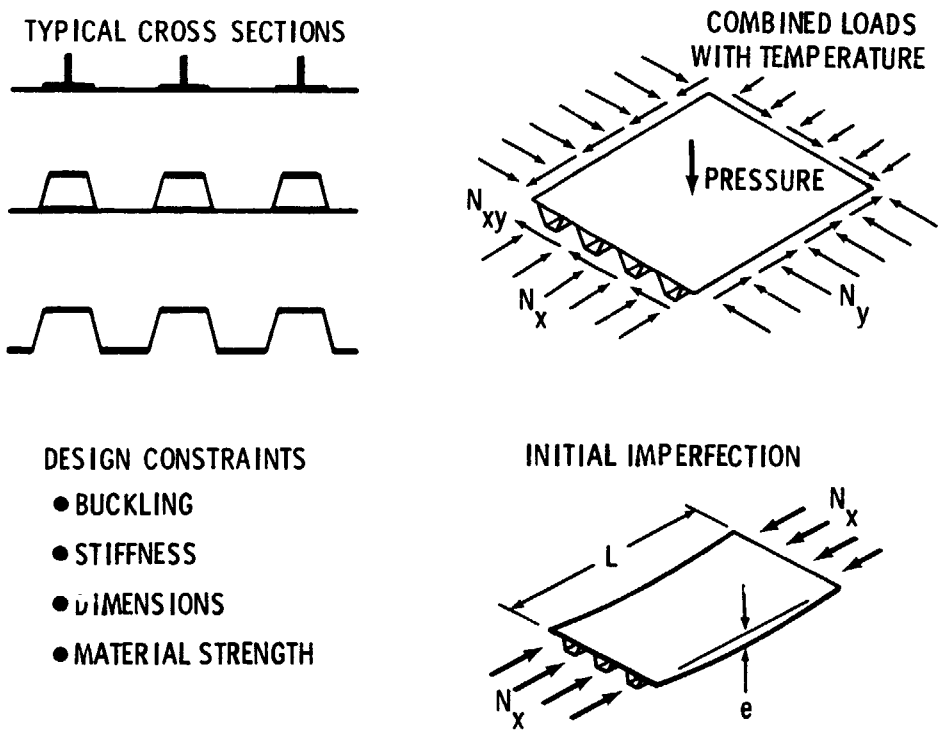

Figure 4.- PASCO panel optimization capabilities.

ORIGINAL PAGE IS OF POOR QUALITY

TABLE II.- PANEL CROSS SECTION DIMENSIONS AND LAYUP PATTERNS.

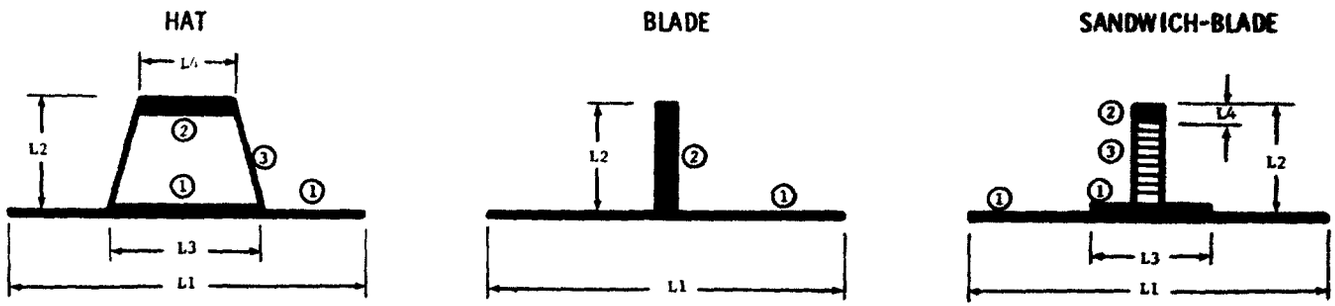

Design	Configuration	Dimensions, cm				No. of Plies at Various Orientation Angles [a]						
						① Skin			② Stiffener			③ Web
		L1	L2	L3	L4	45°	0°	90°	45°	0°	90°	45°
A	Sandwich-Blade	8.53	4.72	3.50	0.75	8 8	0 19	0 0	8	43	0	8
B	Blade	12.70	3.24	-	-	8	2	18	8	4	0	-
C	Blade	11.43	3.38	-	-	12	13	0	4	20	0	-
D	Blade	12.70	3.31	-	-	12	12	0	8	23	0	-
E	Blade	12.70	4.42	-	-	18	5	0	8	42	0	-
F	Blade	11.43	4.58	-	-	18	6	0	8	35	0	-
G	Blade	12.70	5.29	-	-	30	8	3	20	50	5	-
H	Hat	20.32	5.24	7.62	4.68	26	18	4	20	48	4	20
I	Hat	20.32	5.24	7.62	4.68	11[b]	14	4[b]	10[b]	44	4[b]	10[b]

[a]Orientation angle with respect to direction of stiffeners.
[b]Fabric

stiffness, and the 1.21 GPa shear modulus reduces the buckling strain by 19 percent. The NASTRAN solutions and experimental results correlate closely with the reference 5 approximate analysis solutions.

Stiffened Panel Sizing Procedure - PASCO

The VIPASA buckling analysis described in the preceding section has been incorporated in a computerized sizing program denoted PASCO (Panel Analysis and Sizing Code). Some important capabilities of PASCO are indicated in figure 4. The code can be used to size stiffened panels having an arbitrary configuration subjected to any combination of inplane loadings (tension, compression and shear) and lateral pressure. The panel cross section is modeled as an assembly of flat plate elements in which each of the plate elements is a balanced symmetric laminate with an arbitrary number of layers. The panel cross section and loading are assumed to be uniform in the direction of the stiffeners. Stresses associated with a bow-type initial imperfection or lateral pressure are accounted for using a beam-column approach.

During sizing, the merit function is the mass index $\frac{W/A}{L}$, the mass per unit area of the panel divided by the panel length. The sizing variables are the individual plate widths, ply thicknesses, and ply orientations. Inequality constraints can be placed on buckling loads, lamina stresses or strains, and overall panel stiffnesses. The objective of the procedure is to determine the values of the sizing variables which minimize the mass index and satisfy the prescribed set of inequality constraints. Additional discussion of PASCO is presented in reference 8.

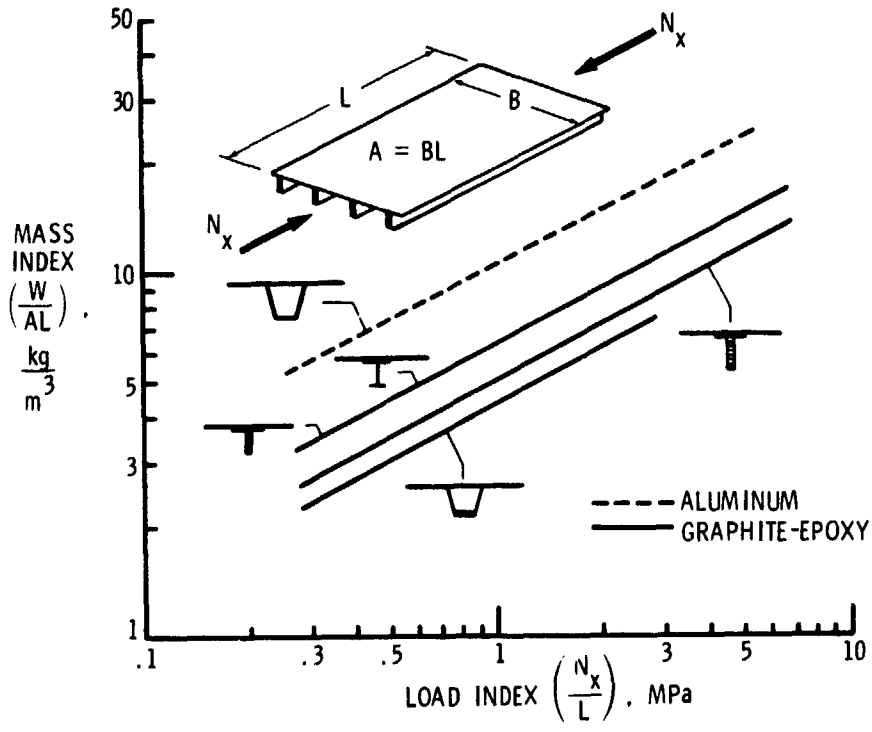

Figure 5.- Structural efficiency of various stiffened panel configurations.

ORIGINAL PAGE IS OF POOR QUALITY

PASCO APPLICATION EXAMPLES

In the two studies presented below denoted "longitudinal compression" and "combined loads", the panels were assumed to be geometrically perfect and the only imposed constraint was buckling. The increases in mass necessary to meet the additional requirements imposed by a geometric imperfection and by prescribed extensional and shear stiffnesses are presented in the section entitled "effect of overall bow and stiffness requirements."

Longitudinal compression.- Structural efficiency data for graphite-epoxy panels with several cross sectional configurations sized to carry only longitudinal compressive loads, N_x, are presented in figure 5. Also shown for comparison is a curve for the minimum mass of hat-stiffened panels constructed of aluminum which was originally presented in ref. 9. The least efficient graphite-epoxy panels are the blade- and I-stiffened panels. These two panel configurations have roughly the same efficiency, and are about 40 percent lighter than aluminum hat-stiffened panels. The curve for panels having a honeycomb sandwich-blade are approximately 20 percent lighter than panels with a solid blade. Because the transverse shear flexibility required for these panels cannot be modeled with the present version of PASCO, sandwich-blade stiffened panels were sized using the analysis of reference 5 which includes the transverse shear effects. Finally, the lightest panels shown are the graphite-epoxy hat-stiffened panels (ref. 8). These panels weigh 60 percent less than aluminum hat-stiffened panels.

Combined loads.- Blade-stiffened panels having the configuration and variables described in reference 8 were sized for pure longitudinal compression and for selected ratios of biaxial compression and shear. The panels were square (76.2-cm-length sides) and were sized to have an integer number of stiffeners. The results are presented in figure 6. The optimum number of stiffeners varies with loading from 16 stiffeners for lightly-loaded panels (0.07 to 0.10 MPa) to eight stiffeners for heavily-loaded panels (5 to 7 MPa).

Effect of overall bow and stiffness requirements.- One type of geometric initial imperfection that is common in panels and that can be accounted for with PASCO is the overall bow-type geometric imperfection. The first-order effect of the bow imperfection is assumed to be the additional stresses produced by bending. In PASCO, these bending stresses are calculated using a beam-column approach and are added to the stresses produced by the inplane loading. The resultant stresses are used to calculate the buckling loads and are also examined for maximum stress and strain limitations.

Panels also commonly have requirements which can be met by imposing limits on stiffness. Several smeared orthotropic stiffnesses are calculated in PASCO and can be used as inequality constraints during sizing. Studies were carried out to determine the effects of a bow imperfection and of extensional and shear stiffness requirements on the mass of minimum-mass blade-stiffened panels. The results are presented in figure 7. The panels have the same configuration as those presented in figure 6 except that all panels have eight stiffeners and no limitation is placed on panel width. The lowest curve is for panels having neither a bow nor a stiffness requirement. The next higher curve is for panels designed for an overall bow of $e/L = \pm 0.003$, where e is the eccentricity at panel midlength, L is the panel length, and the $\pm$ sign means that panels carry the load whether the bow is positive or negative. The highest curve shows the effect of adding shear and extensional stiffness requirements typical of transport aircraft wing panels. The stiffness requirements are taken from reference 1 and are given in Table III. These panels are also assumed to have an overall bow of $e/L = \pm 0.003$. The results indicate that designing for an overall bow of $e/L = \pm 0.003$ causes a mass penalty of about 15 percent and that adding a representative stiffness requirement results in an additional penalty of 18 to 50 percent.

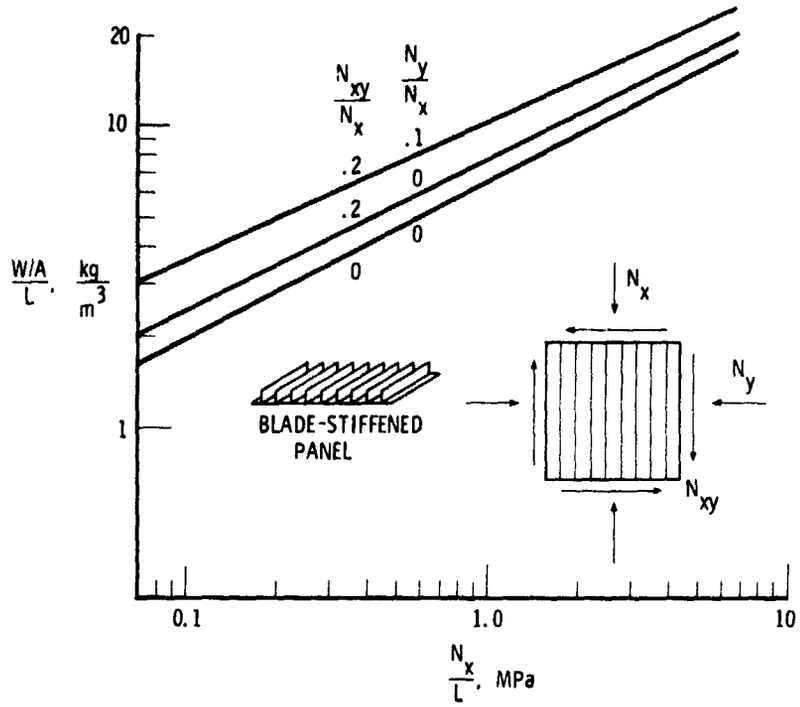

Figure 6.- Structural efficiency of graphite-epoxy blade-stiffened panels designed for specified ratios of combined inplane loads. Panels are square, 76 cm on a side.

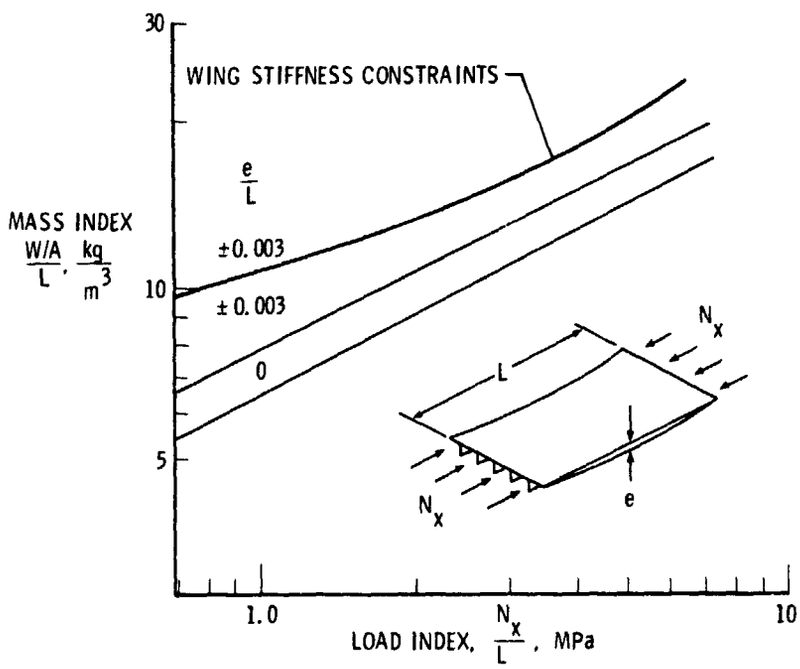

Figure 7.- Effect of selected constraints on the structural efficiency of graphite-epoxy blade-stiffened panels.

TABLE III.- MINIMUM STIFFNESS REQUIREMENTS REPRESENTATIVE OF COMMERCIAL AIRCRAFT WING PANELS.

Loading Intensity N_x/L^a, MPa	Longitudinal Stiffness ET, MN/m	Shear Stiffness GT, MN/m
0.689	386	79
1.720	508	105
3.440	613	133
5.510	701	165

[a]L = 76.2 cm

EXPERIMENTAL BUCKLING AND STRUCTURAL EFFICIENCY STUDIES

Theory-Experiment Buckling Correlation

It is important to understand the accuracy with which the buckling load of a composite panel can be predicted by theory. Discrepancies as high as 40 percent were reported in reference 9. The explanations given for these discrepancies were variations in thickness, variations in material properties from the nominal values used in analysis, and anisotropic and residual thermal stress effects not accounted for in the analysis. Considerable effort is required to conduct an analysis which is sufficiently accurate to permit valid comparisons between experiment and theory. To illustrate some of the important factors which must be considered, a detailed analysis was performed for a blade-stiffened panel loaded to buckling. The panel constructed of graphite-epoxy tape (material A) using design F (Table II) was three stiffeners wide and 76.2 cm long.

The specimen buckled at a load of 1.76 MN/m and axial strain of 0.0037. The corresponding analytical prediction for the panel based on nominal properties and dimensions was a buckling load of 1.52 MN/m and axial strain of 0.0032. The effects that deviations from nominal values have in causing differences between experiment and theory are shown in figure 8. All barred quantities in the figure are associated with nominal material properties and dimensions assumed in the design analysis. The moire-fringe pattern photograph (fig. 8(a)) shows the specimen buckled into four half waves along the length which is in agreement with the theoretical prediction (the fringe pattern for one-half wave is missing in the photograph due to the limited size of the grid).

Two fundamental quantities can be measured experimentally - the imposed strain and the total load. To evaluate a buckling theory, comparing experimental and theoretical buckling strains is useful because the buckling strain is essentially constant with respect

ORIGINAL PAGE IS
OF POOR QUALITY

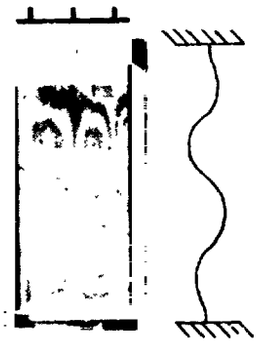

	BUCKLE HALF WAVES
THEORY	4
EXPERIMENT	4

(a) BUCKLING MODE.

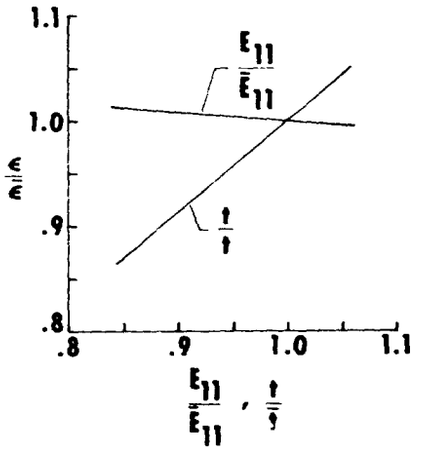

(b) MODULUS AND THICKNESS EFFECT ON STRAIN.

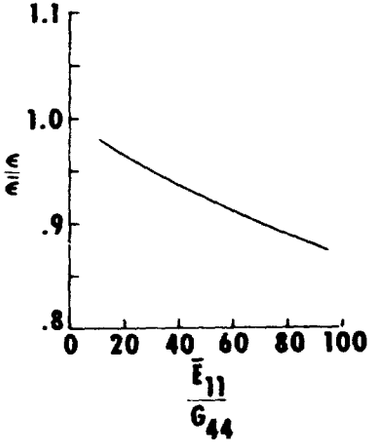

(c) TRANSVERSE SHEAR EFFECT ON STRAIN.

INFLUENCING FACTOR	$\frac{\epsilon}{\bar{\epsilon}}$
NOMINAL PROPERTIES	1.00
MODULUS (FIBER DIRECTION)	1.00
SKIN THICKNESS	0.96
TRANSVERSE SHEAR MODULUS	0.95 TO 0.92
CUMULATIVE EFFECT	0.91 TO 0.88
EXPERIMENT	0.87

(d) FACTORS AFFECTING CORRELATION OF BUCKLING STRAIN.

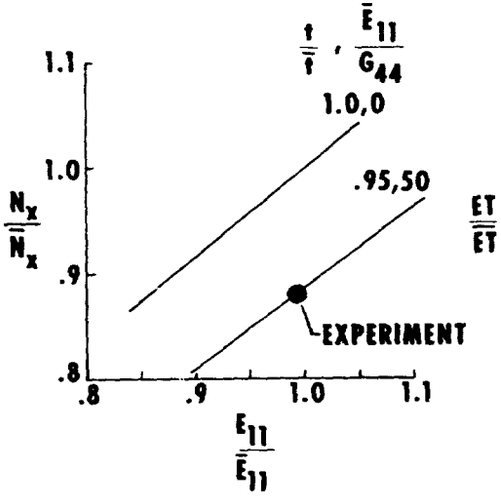

(e) LOAD COMPARISON.

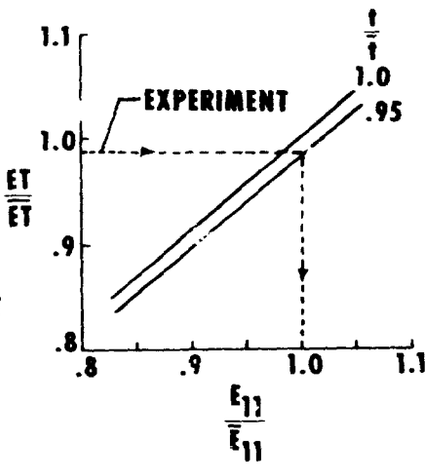

(f) STIFFNESS COMPARISON.

Figure 8.- Correlation of theoretical and experimental buckling of composite panels.

to inplane elastic properties (see fig. 8(b)). In this figure only the dominant material modulus E_{11} was varied while all other moduli properties were held constant at the values shown in Table I. The buckling strain, however, is sensitive to ply thickness variations as shown in the buckling strain versus skin thickness graph of figure 8(b). A thorough survey established that the specimen blade ply-thicknesses were essentially nominal but that the skin ply-thickness was 95 percent of nominal. The skin thickness variation accounts for a four percent reduction in the theoretical buckling strain. Transverse shear deformations of the thick blade-stiffener are responsible for further reductions in the buckling strain as shown in figure 8(c). The value of the transverse shear modulus is not readily available, but considering the properties of the matrix and reported values for inplane shear modulus, it is probably within the range of $\bar{E}_{11}/G_{44}$ from 30 to 60 shown on the plot. Transverse shear, therefore, may account for a five to eight percent reduction in the buckling strain. The cumulative effect on buckling strain of material property and thickness variations from nominal compared to the experimental results is shown in figure 8(d). Correlation of theory and experiment is good when all of these factors are considered collectively, whereas looking at a comparison based on nominal properties would indicate a 13 percent discrepancy.

A fundamental quantity of interest to the structural analyst is the structure buckling load. If the material properties are not accurately known, the actual buckling load may not agree with theory even though the strain is in agreement. The buckling load is a direct function of the material stiffness properties as illustrated in figure 8(e). The upper curve is for the nominal skin thickness and classical theory, and the lower curve is for a reduced skin ply thickness of $t/\bar{t} = 0.95$ and a correction for transverse shear deformation corresponding to $\bar{E}_{11}/G_{44} = 50$.

An indication of the accuracy of the assumed material properties (Table I) can be obtained from comparison of the theoretical and experimental axial stiffnesses shown in figure 8(f). The two theoretical curves are for the nominal skin thickness and a reduced skin ply thickness of $t/\bar{t} = 0.95$ corresponding to the test panel. The experimental stiffness ($ET/\overline{ET} = 0.99$) was obtained from the applied load and the average of several longitudinal strain gage readings. Use of the nominal material properties ($E_{11}/\bar{E}_{11} = 1$) gives excellent correlation between experiment and the lower curve for the test panel ($t/\bar{t} = 0.95$). Small coupon tests of samples cut from the panel also confirmed the selection of material properties. Use of nominal material properties also permit close correlation of theoretical and experimental results for the buckling load (see the lower curve on figure 8(e)). Since the nominal material properties are reasonably accurate for the test panel, the discrepancy between the experiment and theory for buckling load based on nominal properties and classical theory is the same as the discrepancy for strain; namely, 13 percent. These results show that excellent agreement between theory and experiment can be obtained for both strain and load if accurate material and geometric properties and sufficiently precise theory are used.

Other factors which can affect comparison of theory and experiment are boundary conditions and geometric imperfections. For the local buckling mode shown in figure 8, loaded-end boundary conditions effects were small as indicated by a finite element analysis on a similar configuration presented in reference 5. The effect of an overall bow imperfection were also small since the bow imperfection was measured to be small ($e/L = 0.001$). In addition, a bow-type imperfection has a greater effect on the Euler buckling load which was significantly higher than the twisting buckling mode exhibited by this test panel.

Panels Designed to Meet Typical Commercial-Aircraft Wing-Stiffness Requirements

Experiments were conducted on graphite-epoxy panels which were designed to meet not only buckling and strength constraints but also to have extensional and shear stiffness properties typical of commercial aircraft wing structures (See Table III). Five panels (see figure 9) were tested including three blade- and two hat-stiffened panels.

ORIGINAL PAGE IS
OF POOR QUALITY

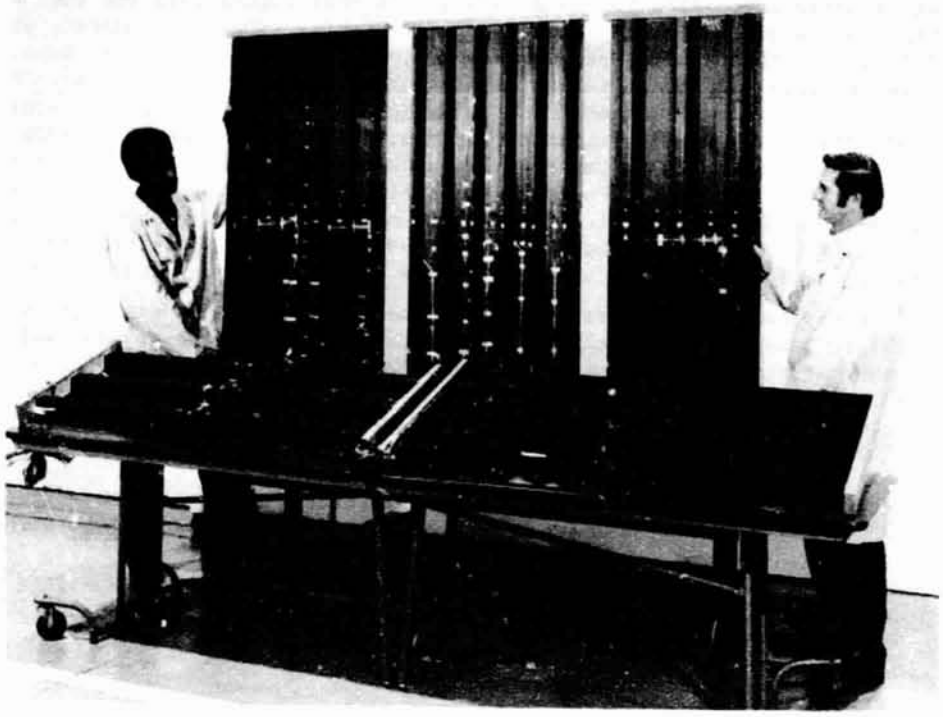

Figure 9.- Hat- and blade-stiffened panels designed to meet commercial aircraft wing stiffness requirements.

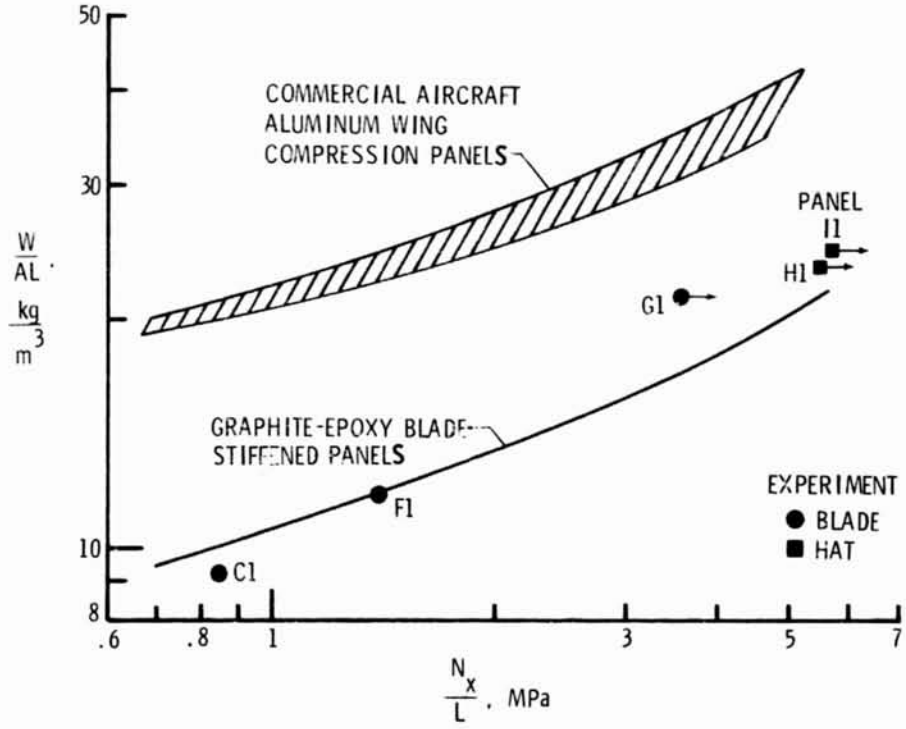

Figure 10.- Structural efficiency of compression panels designed to meet commercial aircraft wing stiffness requirements.

Cross sectional dimensions along with the number and orientation of plies for characteristic elements of the cross section are presented in Table II (designs C, F, G, H and I). Experimental data for the panels are presented in Table IV. The specimens were 1.47 m long which when flat-end tested yielded an effective simple support length of 76.2 cm.

The experimental results for these specimens are plotted on the structural efficiency graph of figure 10. For comparison, the structural efficiency curve for a graphite-epoxy blade-stiffened panel configuration designed to meet bow imperfection and wing-stiffness requirements (reproduced from figure 7) as well as structural efficiency data for typical commercial aircraft aluminum wing panels (taken from reference 1) are presented. Stiffness is such a strong design factor for the load range shown that the theoretical curve for a graphite-epoxy hat-stiffened panel configuration would differ only slightly from that shown for a blade-stiffened configuration. The mass savings for the graphite-epoxy panels compared to the aluminum wing designs range from over 50 percent for the lightly-loaded blade designs to approximately 30 percent for the heavily-loaded designs. The test data for the lightly-loaded panels fall on or below the theoretical curve while the test data for the heavily-loaded panels plot above the curve. Lightly-loaded panels C1 and F1 were loaded until they buckled, which occurred without failure. The heavily-loaded panels G1, H1, and I1 were not buckling critical at the design load, and the tests were terminated at or near the design load to permit the specimens to be used in damage tolerance studies. The arrows drawn on figure 10 indicate the panels have additional load capability.

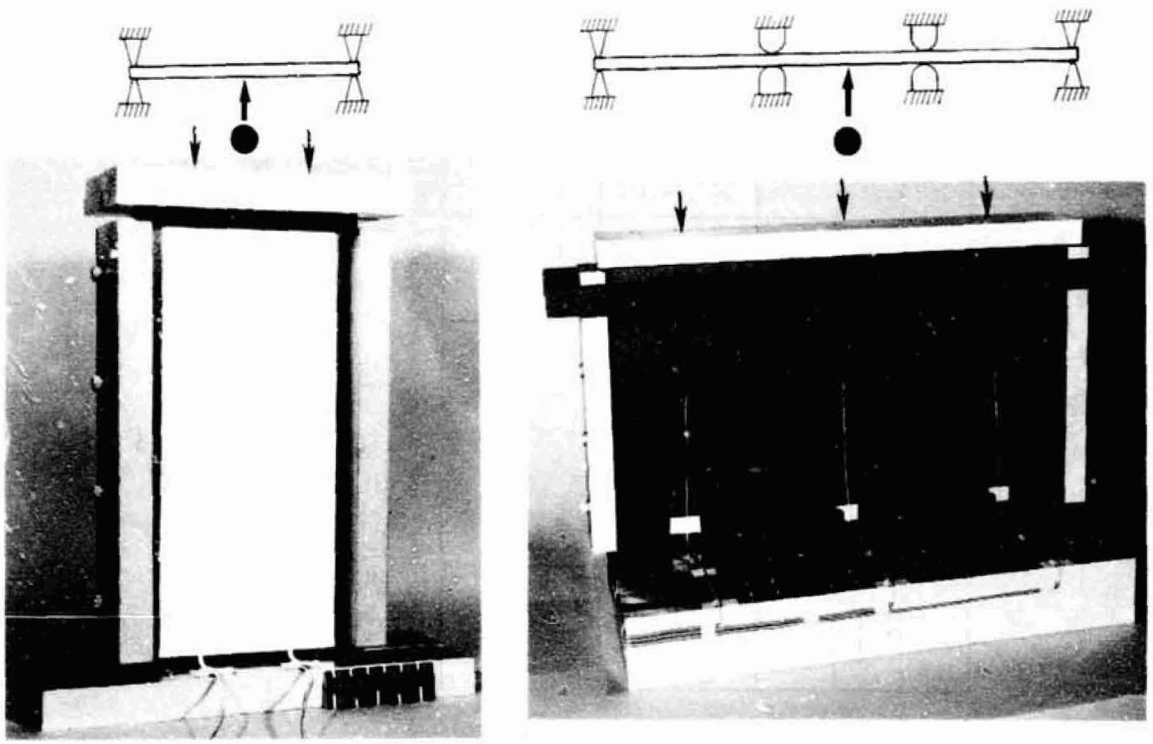

Figure 11.- Laminate specimens in one- and three-bay compression fixtures.

ORIGINAL PAGE IS
OF POOR QUALITY

TABLE IV.- EXPERIMENTAL DATA FOR 1.47-m-LONG PANELS DESIGNED TO MEET COMMERCIAL AIRCRAFT REPRESENTATIVE EXTENSIONAL AND SHEAR STIFFNESS REQUIREMENTS. TEST CONDITIONS SIMULATE 76.2 cm SIMPLE-SUPPORT LENGTH.

Panel			Initial Imperfection		Extensional Stiffness, MN/m	Mass per unit Surface area, kg/m^2	Maximum N_x, MN/m	Average Strain at Max. N_x	Panel Condition at Max. N_x
Number[a]	Configuration and Design	Width, cm	$\frac{e}{L}$	$\frac{\Delta}{B}$					
C1	Blade	76.3	-	-	426	7.08	0.64	0.0015	Buckled
F1	Blade	65.4	-.0010	+.0006	434	8.98	1.06	0.0025	Buckled
G1	Blade	73.0	-.0009	-.0046	723	16.40	2.70	0.0037	Test terminated prior to buckling or failure
H1	Hat	57.2	-.0004	-.0045	720	18.20	4.20	0.0058	Test terminated prior to buckling or failure
I1	Hat	56.9	-	-	732	19.00	4.32	0.0059	Test terminated prior to buckling or failure

[a]Letter indicates design described in Table II.

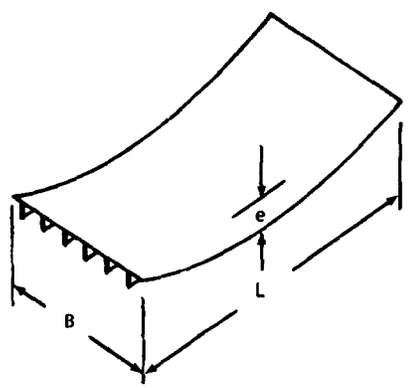

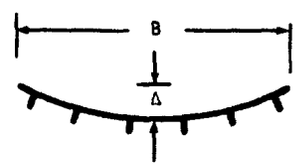

IMPACT-DAMAGE TOLERANCE OF COMPOSITE STRUCTURES LOADED IN COMPRESSION

Structural efficiency studies, such as those presented in the previous section, have demonstrated the mass-saving potential of high-modulus filamentary material for compression panels designed to meet buckling and stiffness requirements. The usefulness of composite materials, however, also depends on their ability to carry loads when subjected to damage sustained during the life of the component. The sensitivity of compression loaded structures to low-velocity impact damage was studied using flat-plate laminates as well as stiffened panels.

Flat Laminates Damaged by Low-Velocity Impact

Test configuration and apparatus.- The two test configurations shown in figure 11 were used to study the effect of low-velocity impact on flat laminates. The single-bay specimen shown on the left is approximately 24.8 cm long and 11.4 cm wide while the three-bay specimen shown on the right is approximately 24.8 cm long and 38.1 cm wide. The loaded ends of the specimen were ground flat and loaded in fixtures that approximated clamped-end conditions. Edge and interior restraints approximated simple-support boundary conditions. The specimen size and edge-support conditions were selected to permit the plate to have a high strain at buckling and therefore permit damage-initiated failure to occur at strains lower than the buckling strain. The projectile used was a 1.27-cm-diameter aluminum sphere that was propelled to impact normal to the specimen at velocities ranging from 30 to 150 m/s. A moire-fringe technique was employed to monitor the panel lateral displacement response during loading. The front surface of the specimens was painted white to enhance the contract of the moire fringes. Specimens were instrumented with at least four strain gages.

Physical characteristics of impact damage.- Specimens were impacted in the single-bay test frame and removed to observe the physical characteristics of damage. Following observation of the front and back surface damage, the specimens were ultrasonically inspected. Several were cross-sectioned through the impacted region and inspected microscopically for interior damage.

Ultrasonic C-scan data and photomicrographs of the cross-section for a 48-ply laminate with a $\{\pm 45/0_2/\pm 45/0_2/\pm 45/0/90\}_{2S}$ stacking sequence are presented in figure 12. Data are shown for specimens impacted at 58 m/s and 95 m/s. Visual inspection showed no front surface damage for either specimen. The specimen impacted at 58 m/s did not develop back surface damage while the specimen impacted at 95 m/s had an outer ply crack on the back surface which extended approximately 3.4 cm. Ultrasonic inspection showed both specimens to have sustained interior damage with the greater affected area associated with the higher velocity (figure 12(a)).

Low power microscopic inspection of the cross sections in the damaged region (figure 12(b)). shows limited damage in the specimen impacted at 58 m/s and extensive damage in the specimen impacted at 95 m/s. High power photomicrographs of the cross sections in the damaged region taken with a scanning electron microscope are shown in figure 12(c). Both specimens exhibit delamination cracks between plies of dissimilar orientation (i.e., 0/90, 0/45, and +45/-45) as well as intraply cracking (through-the-thickness) of 0° and $\pm 45^{\circ}$ oriented plies. Failure appears to propagate by matrix fracture and may be associated with cohesive failures in the matrix or adhesive failures in the fiber-matrix bond. These observations show that low-velocity impact can result in significant laminate interior damage in the vicinity of the impact. Several mechanisms may participate in creating the local damage illustrated in figure 12. The plate deformation response following impact is illustrated in figure 13. On contact, internal stress waves are initiated within the panel which may be responsible for developing local damage. The V-shaped patterns observed in the damaged panel (see figure 13(b)) are similar to the fracture patterns created by stress

ORIGINAL PAGE IS OF POOR QUALITY

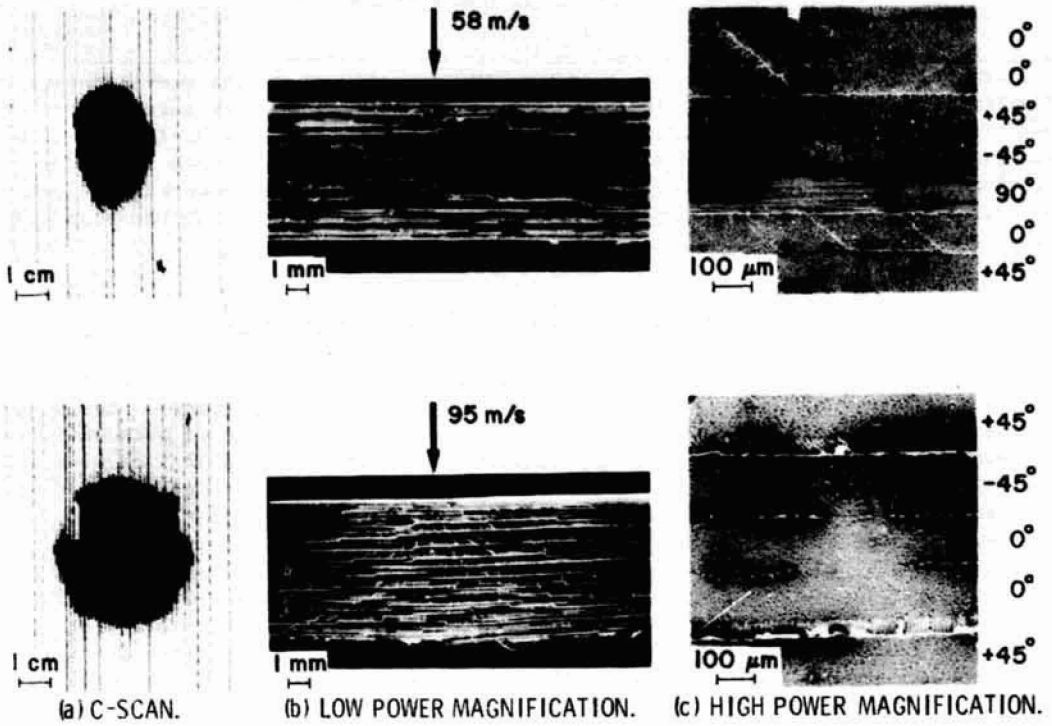

Figure 12.- Interior damage to graphite-epoxy laminates following impact.

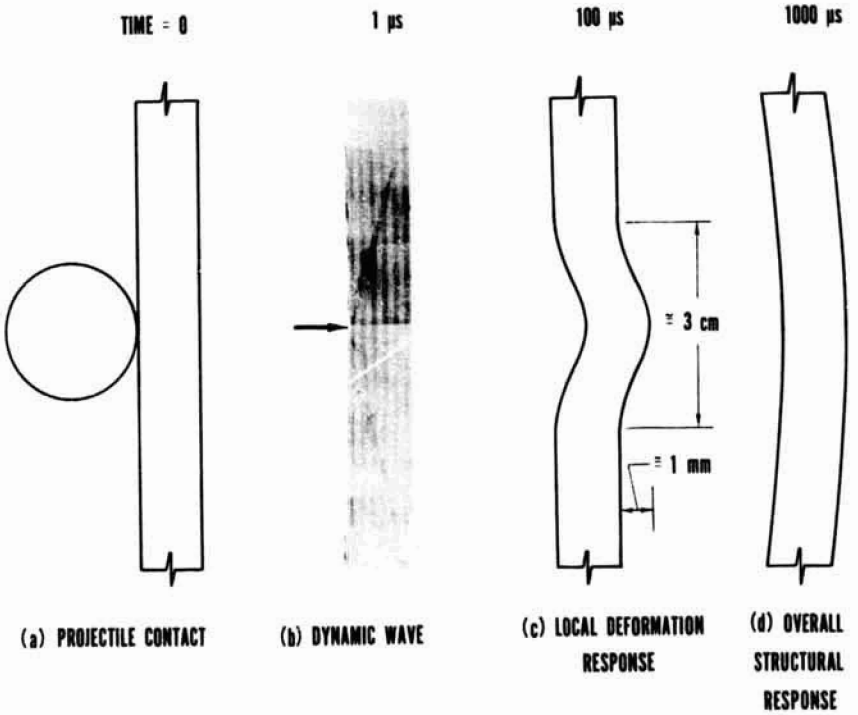

Figure 13.- Deformation response of laminate following low-velocity impact.

waves in homogeneous brittle plates that have been impulsively loaded on one surface. Based on preliminary calculations using bulk material properties, the time required for translations of the initial dynamic wave through the thickness would be on the order of a few microseconds. Once damage has been initiated within the panel, the area in the damaged region has a reduced local stiffness and may deform locally out-of-plane through a combination of stress and local bending of sublaminates. The 48-ply panels impacted at 91 m/s by a 1.27-cm-diameter aluminum projectile had local deformations in the impact damage region that were approximately 3 cm in diameter and a lateral deformation of approximately 1 mm (figure 13(c)). This local out-of-plane deformation may cause damage to propagate or cause additional delamination and intraply cracking to develop. It is anticipated that this local deformation occurs much later in time, probably several orders of magnitude after the initial dynamic wave effects. The out-of-plane deformation due to the plate overall structural response was not measured in this investigation; however, preliminary estimates indicate that it would have occurred later in time (figure 13(d)). The overall structural response probably causes little additional local damage.

Effect of impact damage on strength.- The effect of impact damage on the strength of a 48-ply orthotropic laminate with a $\{\pm45/0_2/\pm45/0_2/\pm45/0/90\}_{2S}$ stacking sequence is reported in reference 10. This information along with additional unpublished test data is presented in figure 14. In these tests, the specimens were impacted while loaded to a prescribed axial strain. Specimens that failed catastrophically on impact are represented by filled circles, and specimens that continued to carry load after impact are represented by open circles. The strain at failure for control specimens are shown for comparison on the ordinate as open circles. Control specimens either failed in the loaded end region or buckled and the test was terminated. The projectile kinetic energy is plotted on the abscissa and discrete projectile velocities are also indicated. The curve labeled "failure threshold strain" in figure 14 separates results of specimens that failed catastrophically on impact from those that did not. The trend of the data indicates the compressive strength of these specimens is affected severely at the higher impact energies. For an impact velocity of 100 m/s, the failure threshold strain was 0.0028.

The test results for the 58 and 95 m/s impact conditions (figures 12 and 14) suggest the extent of interior damage is a key factor affecting the failure threshold strain. Reference 10 indicates a coupling exists between the applied inplane load and the local deformation response associated with impact. This coupling results in a larger local damage region for specimens damaged by impact under load than for specimens which have no applied load at impact.

Additional results are reported in references 10 and 11 of the residual strength of specimens which did not fail on impact. Specimens impacted at zero axial load in the 50 to 60 m/s range were found to have ultimate residual strains significantly higher than the failure threshold strain. Specimen impacted at zero load in the 80 to 100 m/s range, however, were found to have ultimate residual strains only slightly higher than the failure threshold value.

Data presented in figure 14 represents specimens that were both 11.4 cm (single-bay) and 38.1 cm (three-bay) wide. The failure strain and failure mode was unaffected by the specimen width. The damage propagated laterally from the point of impact to the plate edge for both types of specimens. Photographs of failed panels of both specimen sizes are presented in figure 15.

Damage propagation mechanisms.- Three damage propagation mechanisms for compressively loaded laminated composites have been observed. These include: delamination, axial load-lateral deformation coupling, and local shear failure. These propagation mechanisms are illustrated in figure 16. The delamination mechanism (figure 16(a)) can be described as the progressive growth of local interlaminar disbonds during the application of load. The propagation is dependent upon the development of local out-of-plane buckling deformations in the delaminated region. The closer the delaminations are to the surface, the lower is the load required to initiate local buckling. The series of moire-fringe photographs shown

ORIGINAL PAGE IS
OF POOR QUALITY

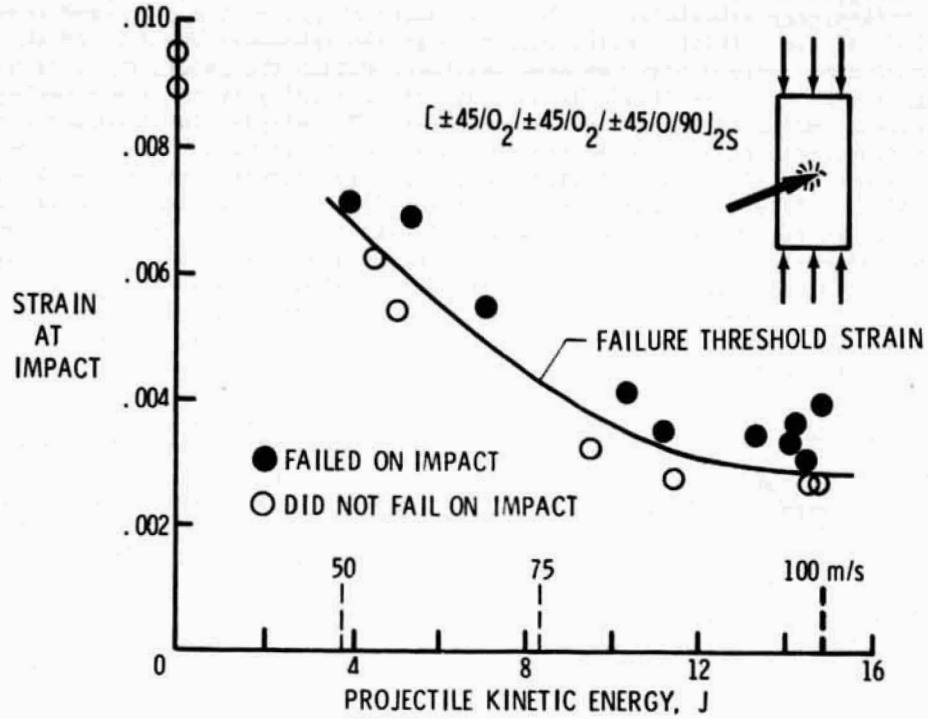

Figure 14.- Effect of impact energy on graphite-epoxy laminate failure strain. Projectiles used were 1.27-cm-diameter aluminum spheres.

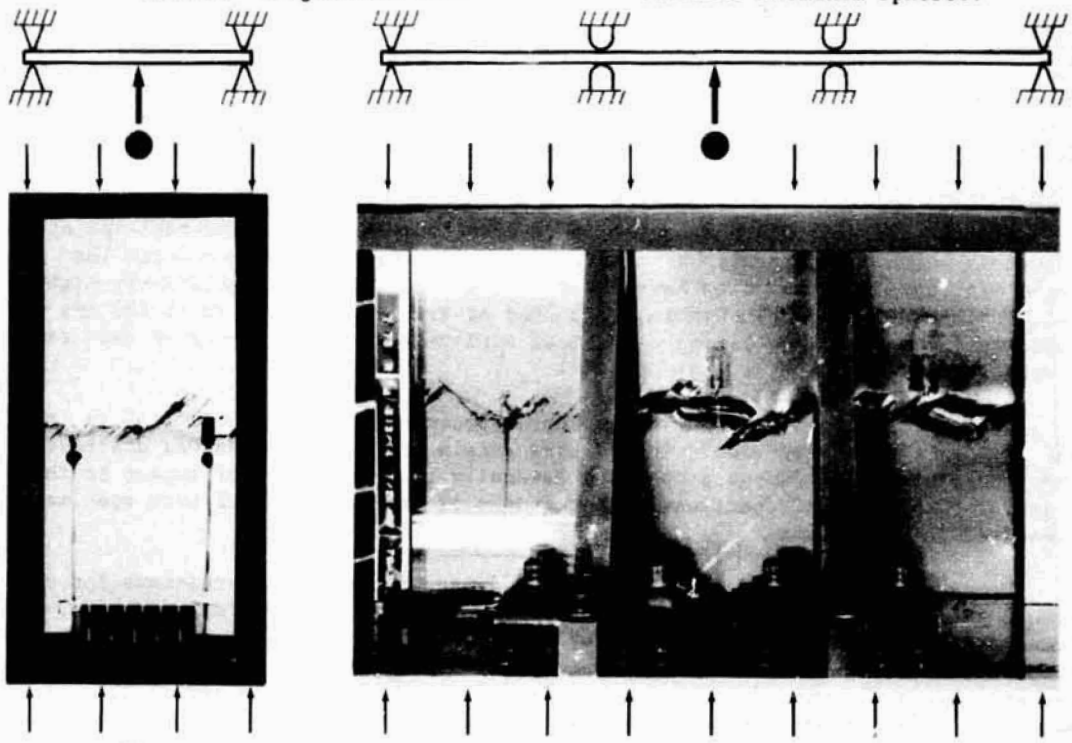

Figure 15.- Photographs of typical failures of impact-damaged graphite-epoxy compression panels.

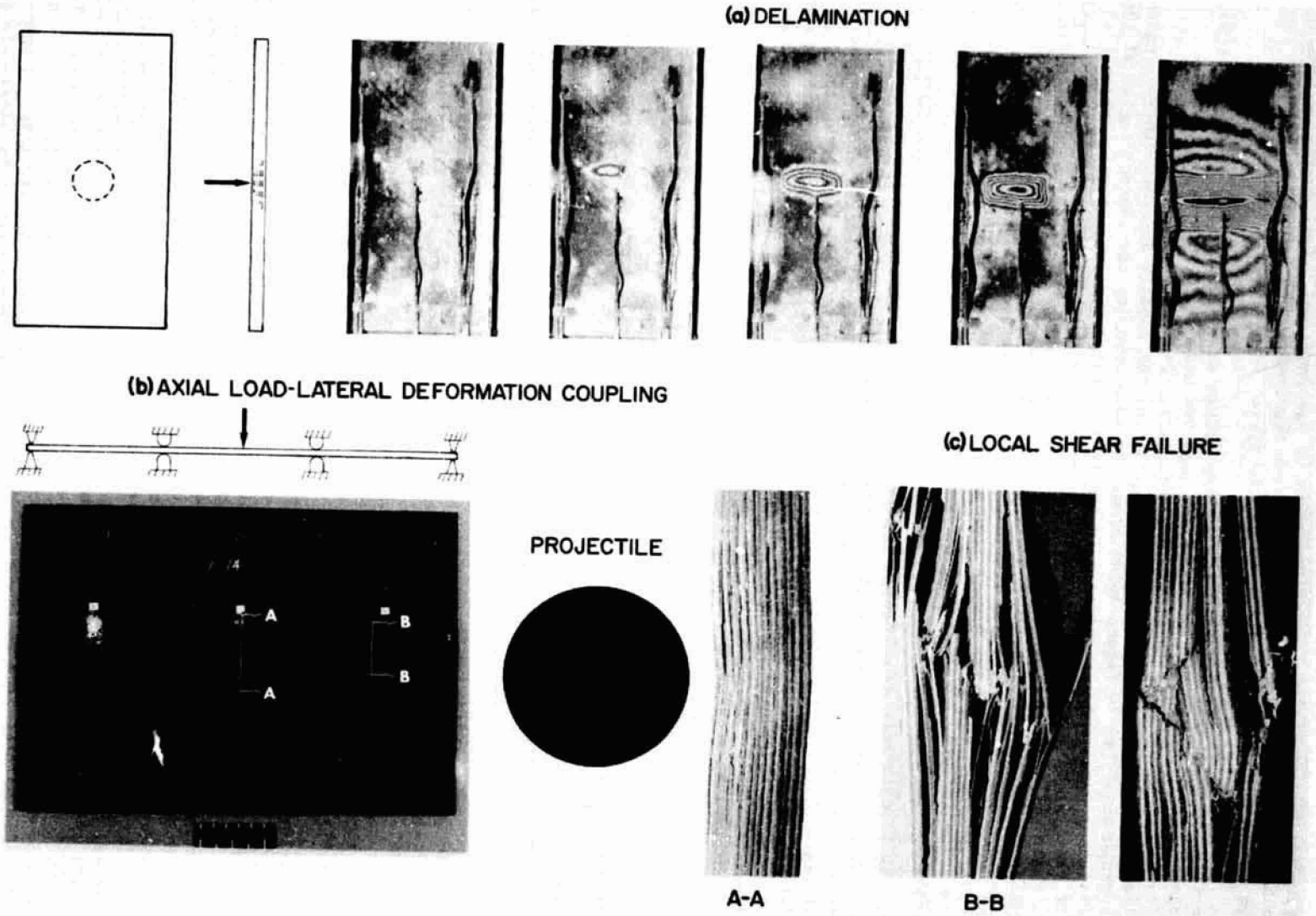

Figure 16.- Damage propagation mechanisms under compression loading.

in figure 16(a) are typical of the progressive delamination growth which occurs with applied load. This failure mechanism is representative of specimens which fail during residual strength tests following impact and has also been observed as the failure propagation mechanism for impact-damaged panels subjected to cyclic compression loads (ref. 10).

The axial load-lateral deformation coupling mechanism is illustrated in figure 16(b). This propagation mechanism occurred in panels impacted under load at strains near the failure threshold value. The local lateral deformation caused by impact, interacts with the applied axial load to cause lateral propagation of the locally deformed damaged region. The photograph presented in figure 16(b) shows the side opposite the contact region of the failed three-bay panel shown previously in figure 15. Cross section A-A taken through the center of the failed region is shown on the right along with the 1.27-cm-diameter projectile drawn to scale. The local deformation in the impact zone and the extensive delamination in the laminate may be seen in the cross section. The interior supports of the test fixture for the panel shown in figure 16(b) restrained the panel lateral deformations and, therefore, arrested the propagation of the damage zone as an axial load-lateral deformation coupling mechanism. The failure, however, propagated through the interior support region and to the panel edges by a shear failure mechanism.

The local shear failure mechanism involves short-wavelength transverse-shear failure such as that illustrated in figure 16(c). The photograph on the left is a cross section from the outer bay of the panel shown in figure 16(b). The cross section shown on the right of figure 16(c) is from another specimen and illustrates more clearly the local shear failure mode. The damage propagation mechanism observed for a typical graphite-epoxy specimen is a combination of delamination and local shear. If the specimen is loaded near the failure threshold during impact, the failure also involves the axial load-lateral deformation coupling mechanism.

Effects of Holes

Tests were conducted on specimens containing an open circular hole to permit comparison of the effect of impact with that resulting from a controlled damage. Detail results of the study are reported in reference 10. The specimens had a $\{\pm45/0_2/\pm45/0_2/\pm45/0/90\}_{2S}$ stacking sequence with hole diameters ranging from 0.16 to 3.81 cm and corresponding diameter-to-width ratios ranging from 0.014 to 0.33. The effect of hole diameter on failure strain is presented in figure 17.

The specimen with a 0.16-cm-diameter hole failed away from the hole at an axial compression strain on the same order as control specimens. Specimens with larger hole diameters failed at strains significantly lower than control specimens. For example, the specimen with a hole diameter of 3.81 cm failed at an axial strain of 0.0038. The failure threshold strain for the same laminate damaged by impact at 100 m/s by a 1.27-cm-diameter aluminum projectile was 0.0028 (see figure 14).

A photograph of a failed specimen with a 1.91-cm-diameter hole is shown in figure 18(a). At an applied strain value of approximately 95 percent of ultimate, local delamination was observed at the hole edge. This delamination continued to propagate laterally to the plate edges with increasing load. A cross section through the hole illustrates that massive delamination occurred in these graphite-epoxy specimens. For comparison, a photograph is presented in figure 18(b) of a 0.64-cm-thick 7075 aluminum plate also containing a 1.91-cm-diameter hole. The 11.4 cm by 24.8 cm aluminum specimen buckled at an axial stress of 540 MPa. This value approaches the ultimate stress for this aluminum material and indicates the hole had negligible effect on reducing the specimen strength. A cross section through the center of the aluminum specimen is shown in figure 18(b). An increase of approximately 11 percent in the thickness was observed locally in the region adjacent to the hole. The ductility of aluminum permits large local deformations to occur in this high stress concentration region without causing catastrophic failure. In comparison, the graphite-epoxy specimen lacks ductility and responds to the local stress concentration by local delamination and specimen failure.

ORIGINAL PAGE IS OF POOR QUALITY

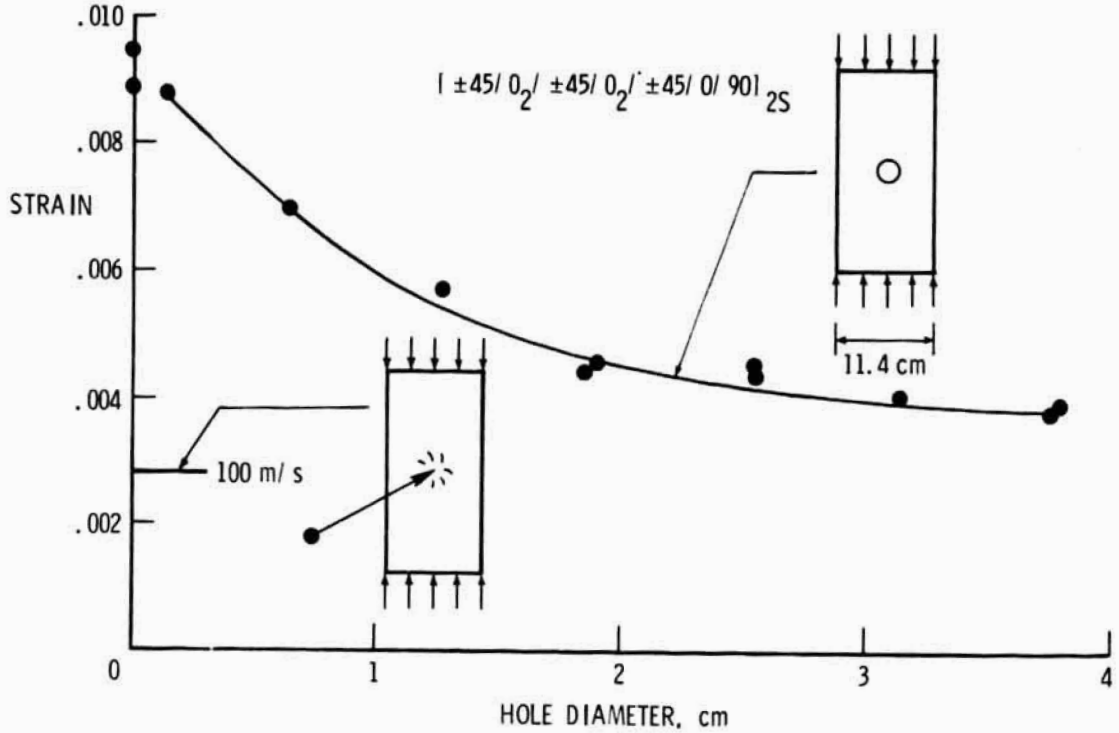

Figure 17.- Effect of holes and 100 m/s impact on the compression strength of a graphite-epoxy laminate.

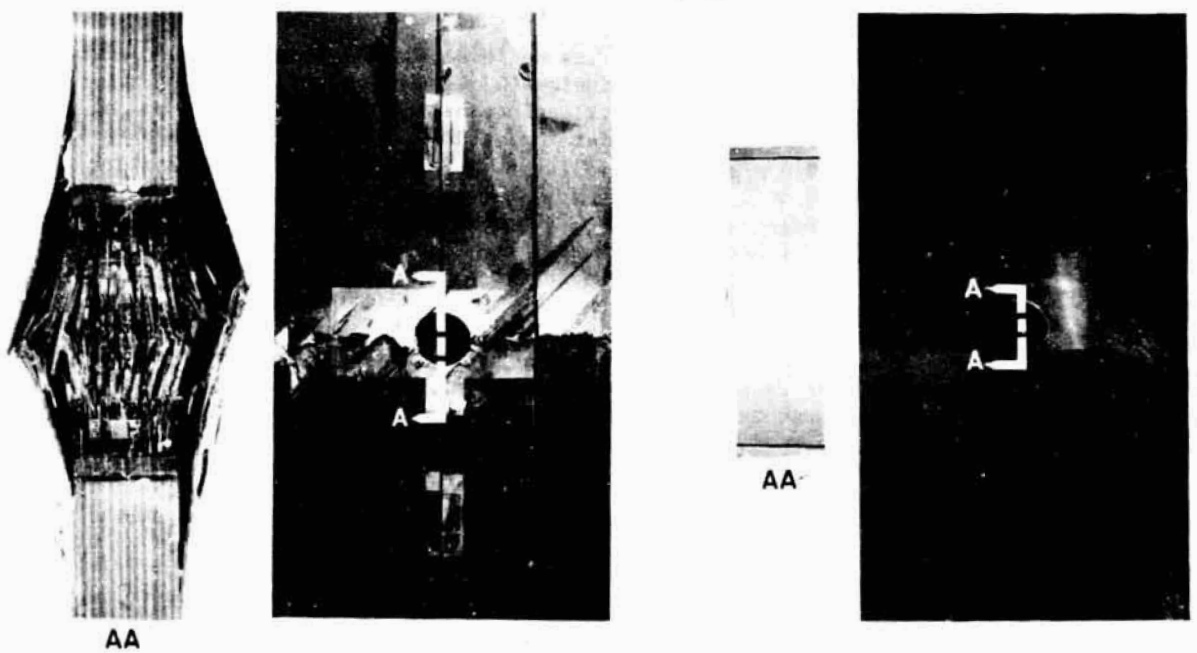

(a) GRAPHITE-EPOXY. (b) ALUMINUM.

Figure 18.- Photographs of graphite-epoxy and aluminum specimens containing a 1.9-cm-diameter hole loaded in compression to failure.

Stiffened Panels Damaged by Impact

The strength of structurally-efficient hat-stiffened panels damaged by impact is reported in references 12 and 13. The study indicated that the influence of impact damage on ultimate strength may be negligible for lightly- to moderately-loaded panels but can be pronounced for heavily-loaded panels designed to carry loads at high strains. The present paper reports additional damage tolerance studies on compression panels designed to carry compression loads without buckling and to match the extensional and shear stiffnesses of typical commercial aircraft wing panels. The stiffness requirement results in designs which are heavier than those required to meet buckling requirements alone. The present experimental studies included lightly- and heavily-loaded blade-stiffened panels as well as heavily-loaded hat-stiffened panels.

A photograph of the experimental apparatus is shown in figure 19. Specimens were proof tested to the design load to ensure panel integrity. Some specimens were impacted with no applied axial load and then loaded in compression to obtain their residual strength, while other specimens were impacted while loaded. Some loaded panels that did not fail catastrophically upon impact were subsequently loaded to failure to obtain their residual strength.

Test parameters and results of this study are presented in Table V and a summary of the test data on the effect of low-velocity impact damage on the ultimate strain of stiffened panels loaded in compression is presented in the bar graph of figure 20. Selected data taken from reference 13 are also shown in figure 20. The designs range from lightly-loaded (.53 MN/m) panels to heavily-loaded (5.8 MN/m) panels. The horizontal dashed lines in figure 20 represent the theoretical buckling strain at the indicated design load and a hat or blade symbol is above multiple test data of a corresponding design. The solid circles indicate the applied axial strain at the time of impact. If a panel failed on impact, the circle is at the top of the bar. If a panel did not fail on impact, the bar extends above the solid circle to the failure strain measured during the residual strength test.

Blade-stiffened panels.- Strength tests on impact-damaged panels were conducted on blade-stiffened specimens constructed of designs D, E, and G (Table II). Lightly-loaded specimens D1, E1, and E2 exhibited postbuckling capability without failure during proof tests. Specimen D1 was impacted while under load at two locations between stiffeners at velocities of 101.0 and 99.6 m/s without failure. The axial strain at impact for these two tests was 0.0015 and 0.0020, respectively. Extensive back surface damage was inflicted as can be seen in the photograph of panel D1 shown in figure 21(a). The damaged panel was capable of carrying a load in the postbuckled state that was approximately 28 percent greater than the undamaged panel buckling load. A photograph of the moire-fringe pattern illustrating the skin buckle pattern is shown in figure 21(b). Test results for specimens E1 and E2 indicate these lightly-loaded panels were also unaffected by these impact damage test conditions. Specimen E2 sustained complete penetration by the projectile and was capable of carrying a load 24 percent greater than the panel buckling load. These test results and results reported in references 12 and 13 indicate the ultimate strength of lightly-loaded panels designed to carry load at relatively low strains (less than 0.003) are essentially unaffected by low-velocity impact damage of the type studied.

Results for heavily-loaded blade-stiffened specimens (design G) indicate the ultimate strength of these panels was degraded by impact at velocities around 100 m/s. During proof tests, design G panels were subjected to loads as high as 4.91 MN/m (strain = 0.0068). Following impact at 61.0 m/s at zero load, panel G2 carried a load of 5.59 MN/m (strain = 0.0075) without failure. Further impact in the adjacent bay at 92.4 m/s at zero load, however, caused the panel to fail at 3.94 MN/n axial load (strain = 0.0052).

Panel G4, impacted at 100.0 m/s while loaded to 2.62 MN/m (strain = 0.0035), had a residual strength of 2.79 MN/m which corresponds to an axial strain of 0.0037. The panel failed by delamination of the skin with stiffeners remaining undamaged. The series of

ORIGINAL PAGE IS
OF POOR QUALITY

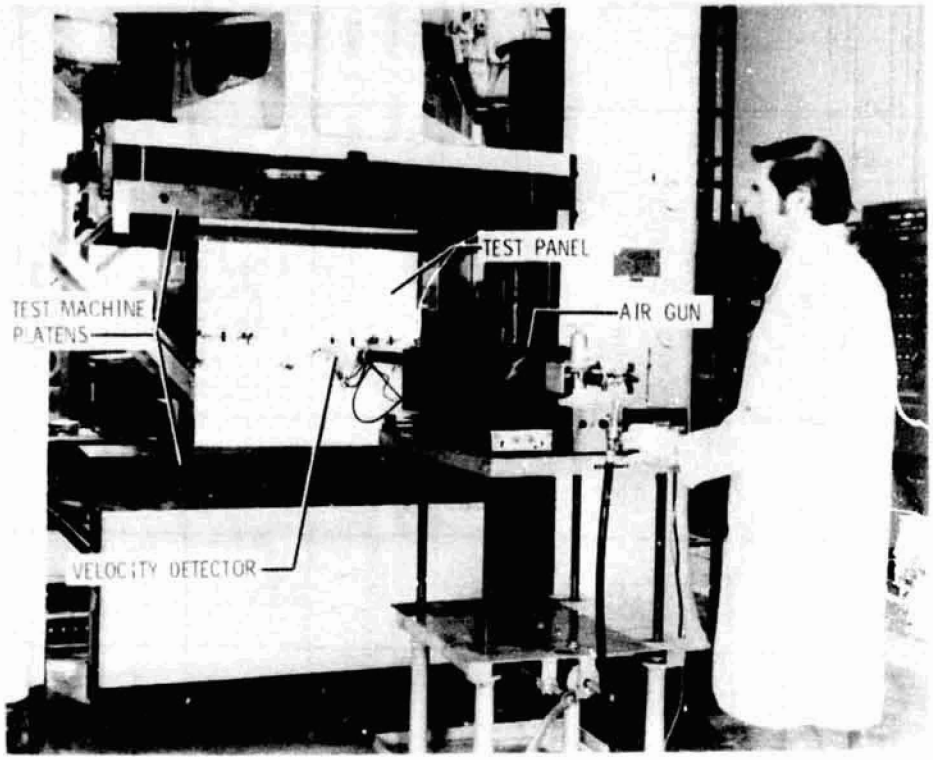

Figure 19.- Apparatus for impacting compression panels under load.

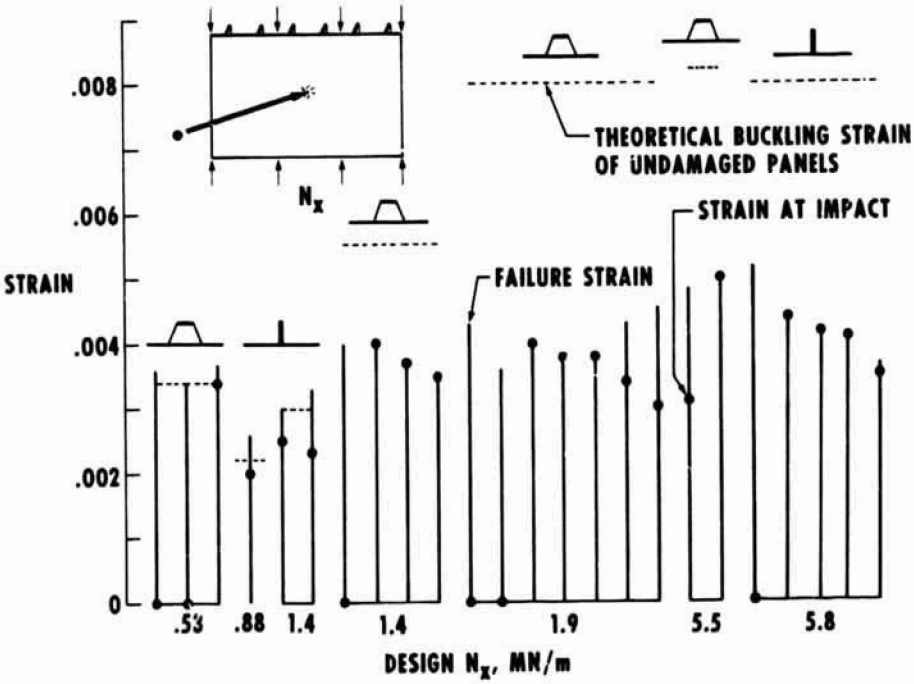

Figure 20.- Strain at failure for impact-damaged graphite-epoxy compression panels.

TABLE V.- THE EFFECT OF IMPACT-DAMAGE ON COMPRESSION PANEL STRENGTH.

(a) Blade-Stiffened Panels

PANEL			PROOF TEST		IMPACT TEST DATA[a]					RESIDUAL STRENGTH	
Number[b]	Length, cm	Width, cm	Maximum Nx, MN/m	Maximum Strain	Velocity, m/s	IMPACT LOCATION	Nx at Impact, MN/m	Strain at Impact	RESULT	Nx, MN/m	Strain
D1	74.7	33.4	0.87[c]	0.0022	101.0	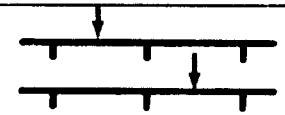	0.59	0.0015	Local damage-no propagation	-	-
					99.6		0.80[c]	0.0020	Local damage-no propagation	1.03[d]	-
E1	30.5	30.7	1.39[c]	0.0030	64.0	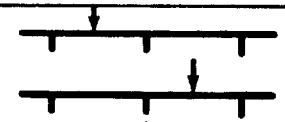	0.95	0.0019	Local damage-no propagation	1.45[c]	0.0031[c]
					51.5		1.25	0.0025	Local damage-no propagation	-	-
					50.6		1.25	0.0025	Local damage-no propagation	1.42[c]	0.0030[c]
E2	17.8	31.2	1.38[c]	0.0031	119.0	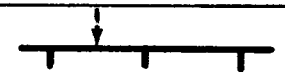	1.22	0.0023	Projectile Penetration-no propagation	1.71[d]	-
G2	51.0	34.3	4.22	0.0056	61.0	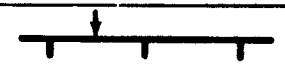	0	0	No visible damage	3.59[c]	0.0075[c]
					92.4		0	0	Local damage-no propagation	3.94	0.0052
G3	51.6	34.3	3.89	0.0052	63.1	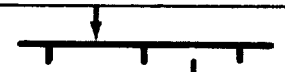	3.11	0.0041	No visible damage	-	-
					97.2		3.11	0.0041	Skin damage propagated to panel edges leaving stiffeners to carry Nx=2.59MN/m	-	-
G4	48.1	36.6	3.93	0.0053	100.0	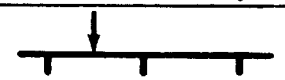	2.62	0.0035	Local damage-no propagation	2.79	0.0037
G5	48.5	36.3	4.32	0.0060	67.7		3.09	0.0042	Catastrophic failure on impact	-	-
G6	48.3	36.5	4.91	0.0068	101.0		3.25	0.0044	Catastrophic failure on impact	-	-

[a]Projectile used was 1.27-cm-diameter aluminum sphere.

[b]Letter indicates design described in Table II.

[c]Buckled without failure.

[d]Major post buckling deformations at failure.

ORIGINAL PAGE IS OF POOR QUALITY

TABLE V. - Continued.

(b) Hat-stiffened panels.

PANEL			PROOF TEST		IMPACT TEST DATA[a]					RESIDUAL STRENGTH	
Number[b]	Length, cm	Width, cm	Maximum Nx, MN/m	Maximum Strain	Velocity, m/s	IMPACT LOCATION	Nx at Impact, MN/m	Strain at Impact	RESULT	Nx, MN/m	Strain
H2	48.8	57.2	4.05	0.0056	96.9		2.29	0.0031	Local damage-no propagation	3.54	.0047
H3	48.8	57.2	4.05	0.0056	96.0		3.59	0.0050	Catastrophic failure on impact	-	-
H4	48.8	57.2	4.05	0.0056	97.2		2.99	0.0042	Local damage-no propagation	-	-
I2	48.8	57.2	4.06	0.0055	97.5		3.01	0.0040	Local damage-no propagation	-	-
I3	48.8	57.2	4.06	0.0055	102.0	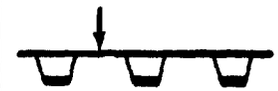	3.01	0.0040	Local damage-no propagation	-	-
					100.0	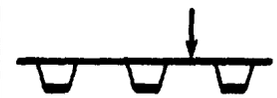	3.24	0.0042	Local damage-no propagation	-	-

[a]Projectile used was 1.27-cm-diameter aluminum sphere.

[b]Letter indicates design described in Table II.

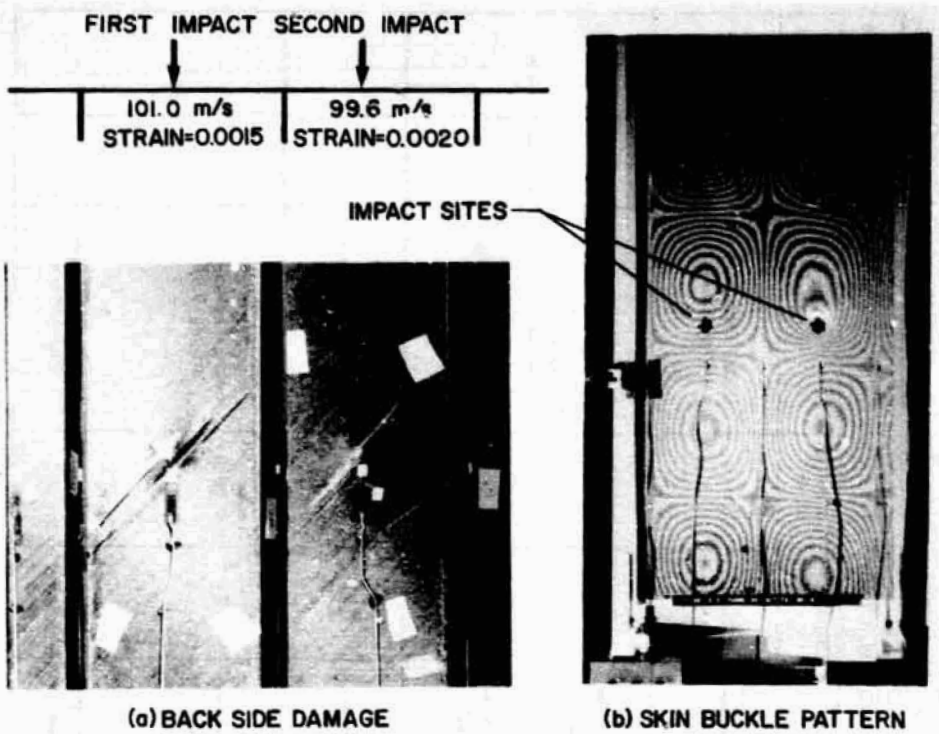

Figure 21.- Post buckling of a lightly-loaded blade-stiffened panel with impact damage.

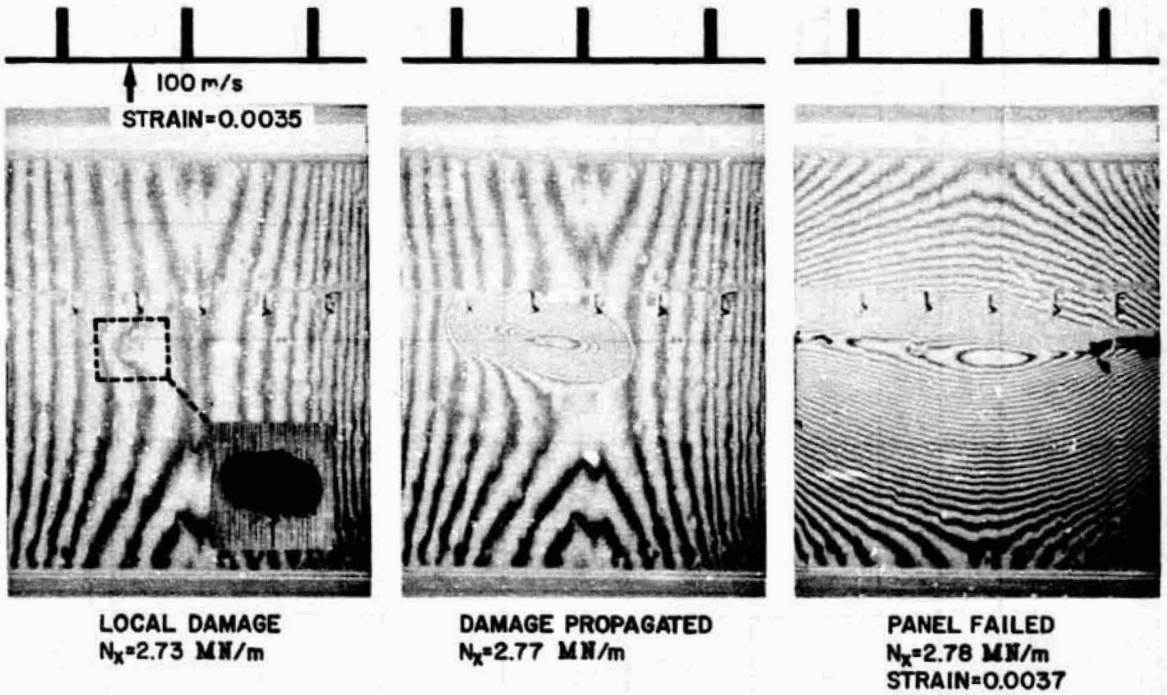

Figure 22.- Propagation of impact damage with load.

ORIGINAL PAGE IS
OF POOR QUALITY

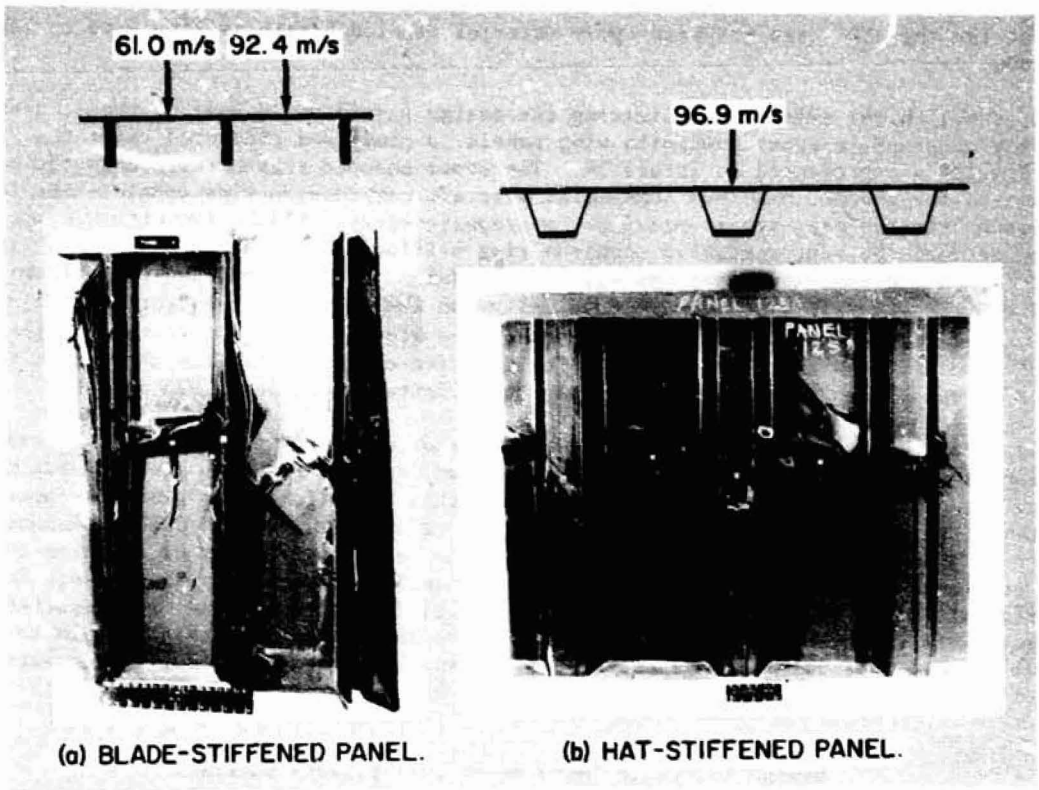

Figure 23.- Ultimate failure of heavily-loaded panels damaged by impact.

three moire-fringe photographs shown in figure 22 illustrates the progressive propagation of the failure boundary which occurred as the load approached the ultimate value. The inset on the first photograph shows the C-scan of the damaged panel taken prior to the residual strength test. The C-scan indicated a damage region approximately 6.3 cm by 3.4 cm. The failure of panels G2, G5 and G6, involved delamination of the stiffeners as well as the skin. A photograph of panel G2 following failure is shown in figure 23(a). Based on these test results, design G impact-damaged specimens have a failure threshold strength and strain of about 2.79 MN/m and 0.0037, respectively.

Hat-stiffened panels.- Impact-damage strength tests were conducted on heavily-loaded specimens of designs H and I (Table II). No significant differences were observed in the failure load of impact-damaged panels of design H (all tape) and design I (mixed tape and fabric). Prior to impact testing, panels of both designs were proof loaded to an axial load of 4.05 MN/m and axial strains of 0.0055. For these hat-stiffened panels damaged by impact at approximately 97 m/s, the failure threshold strength and strain respectively, were greater than 2.99 MN/m and 0.0042 (see Table V(b)). A photograph of panel H2 following failure is presented in figure 23(b). The failure initiated in the impact region and involved delamination and shear failure of the skin as well as destruction of the stiffeners.

Effect on Structural Efficiency of Limiting Ultimate Design Strain

Pending improvements in the damage tolerance of composite structures and the development of better analytical failure prediction techniques, limiting the ultimate design strain appears to be the most effective means for insuring the integrity of composite structures. Although test data are insufficient to establish an accurate limiting strain,

ORIGINAL PAGE IS
OF POOR QUALITY

the value for the 450K cure graphite-epoxy material studied herein is likely to be less than 0.004.

To establish the effect that limiting the design strain would have on the structural efficiency of graphite-epoxy composite wing panels, a study was conducted using the PASCO code. Results are presented in figure 24. The cross-hatched region represents the mass requirements for current aluminum commercial aircraft compression wing panels. The lower curve represents the mass requirements for a graphite-epoxy, blade configuration designed to meet the representative aluminum wing stiffnesses listed in Table III. The graphite-epoxy designs also carry the axial compression loads without buckling assuming an initial bow-type imperfection ($\xi_i = \pm.003$). Although the lower curve had no upper limit on strain, a value of 0.0093 was the highest calculated strain required for the load index range studied. Curves are also presented for graphite-epoxy panels with these same constraints except the maximum axial strain has been limited to either 0.003 or 0.004.

For a value of N_x/L of 0.7 MPa, a mass savings of nearly 50 percent is predicted for the graphite-epoxy design compared with the aluminum design. For N_x/L equal to 5.0 MPa, mass savings of approximately 45, 30, and 15 percent are predicted for graphite-epoxy designs with no limiting strain and maximum strain values of 0.004 and 0.003, respectively. Considering the complete wing compression cover, the total mass effect of limiting the design strain is an accumulative effect found by considering the mass requirements for all the different loads and regions of the wing. Results for one such study are reported in reference 14 in which it was found that limiting the graphite-epoxy design strain to values of 0.004 and 0.003 resulted in mass savings of 26 and 19 percent, respectively, compared to the aluminum designs.

Damage Tolerance Improvement by Alternate Matrix

The mechanisms of damage initiation and failure propagation usually involve matrix failure either through delamination or intraply matrix fracture. The implied matrix dependency suggests increased damage tolerance may be achieved by use of an alternate matrix material. A preliminary survey of commercially available epoxy preimpregnated materials identified one possible epoxy candidate. The effect of impact damage on the strength of this material was studied using plate specimens constructed of a 48-ply $\{\pm45/0_2/\pm45/0_2/\pm45/0/90\}_{2S}$ laminate. The laminate and test conditions permit direct comparison of this graphite-epoxy (material B) with the graphite-epoxy (material A) data presented earlier, since the same graphite fiber was used in both materials. Lamina material properties for material B are listed in Table I. Laminates of material B were 18 percent thicker than laminates of material A, primarily due to the higher resin content (38 percent versus 28 percent).

Results of this investigation are presented in the strain versus impact energy graph of figure 25. Data for material A is reproduced from figure 14. As before, solid symbols represent specimens loaded to the indicated strain that failed on impact, and open symbols represent the strain applied to specimens that did not fail on impact. The failure threshold strain is substantially higher for material B. For example, the failure threshold strain for a 100 m/s impact speed is 0.0028 for material A compared with 0.0062 for material B.

It is important to establish the material properties that affect laminate damage tolerance. Some insight may be obtained by studying the neat-resin tensile properties. Neat-resin tensile properties for materials A and B are shown in the inset of figure 25. Material A has a slightly higher tensile modulus (4.0 GPa versus 3.1 GPa for material B). The ultimate strength of material B is approximately twice that of material A and the strain at failure is approximately four times as great. Studies conducted on matrix materials with tensile stress-strain characteristics similar to those of material B indicate additional properties such as shear modulus and strength, resin content, and strain rate sensitivity may also be important factors affecting the damage tolerance of composite structures.

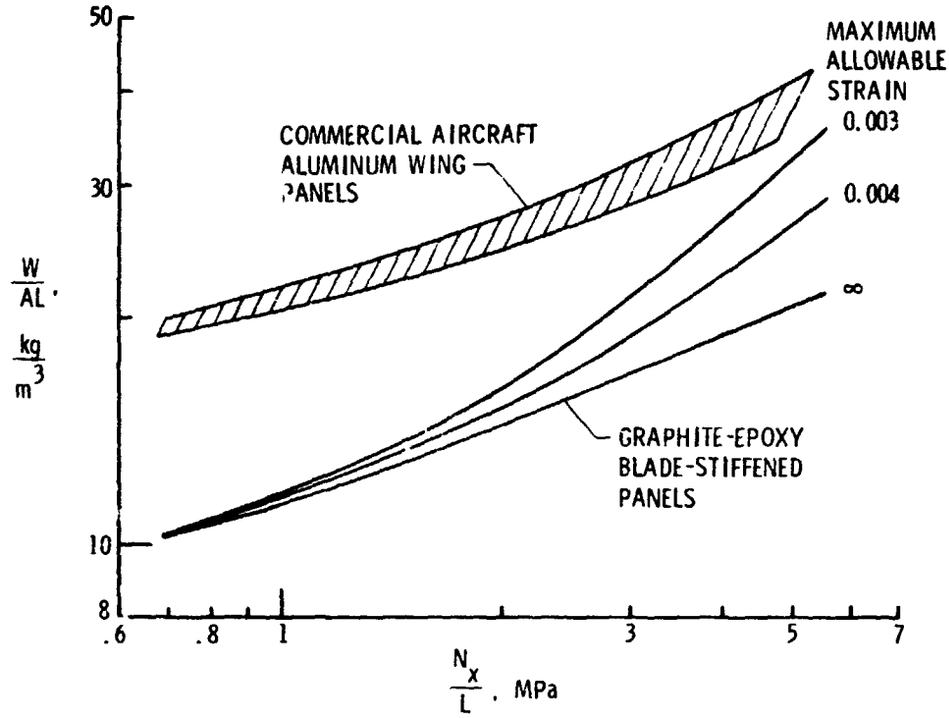

Figure 24.- Effect of limiting strain on structural efficiency of graphite-epoxy wing panels and comparison with aluminum wing panels.

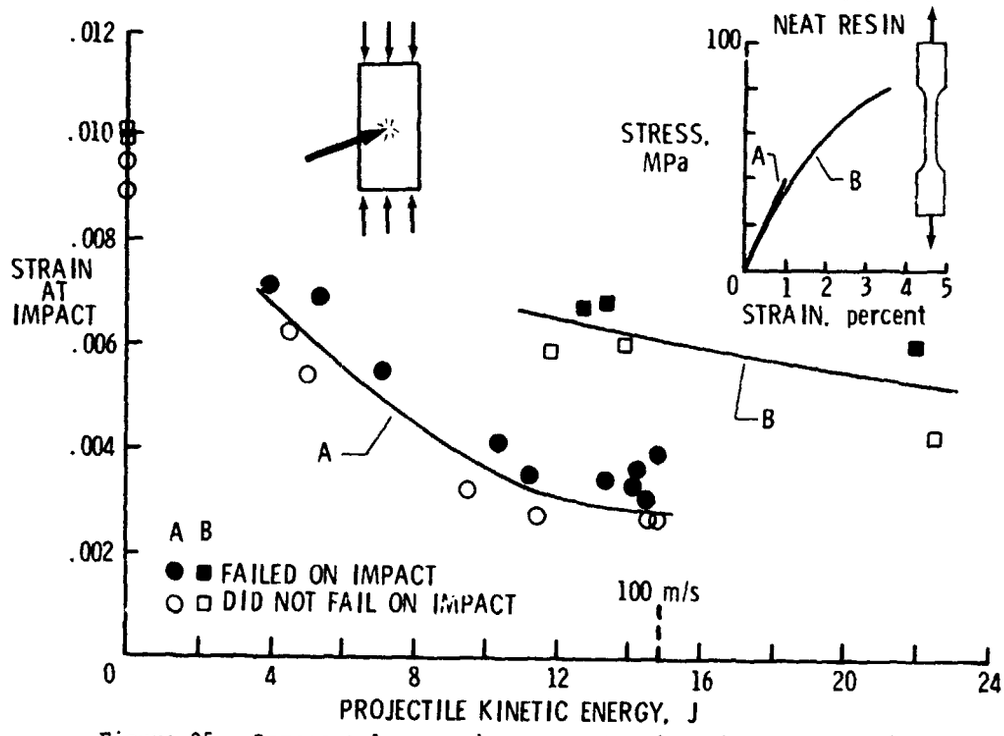

Figure 25.- Damage tolerance improvement using alternate matrix. Projectile used was 1.27-cm-diameter aluminum sphere.

CONCLUDING REMARKS

To achieve the maximum potential structural efficiency for composite panels, a thorough understanding of the factors that affect structural performance including buckling and material strength is required. Recent advances in analysis and sizing procedures reported herein permit composite panel designs to satisfy buckling requirements with greater accuracy and therefore improved structural efficiency. The effect of transverse shear deformations has been included to improve the accuracy of the buckling analysis for sandwich-blade-stiffened panels. A correction factor (based on infinitely wide orthotropic plate solutions) has been applied to improve the solution accuracy for low wave-number inplane shear buckling. Furthermore, a stiffened panel sizing code called PASCO has been developed that uses accurate analyses for buckling and an efficient optimization algorithm for rapid sizing. Additional analysis refinements allow PASCO to account for bow-type initial imperfections, lateral pressure, and thermal effects. The code is used to illustrate the effects that selected configurations, loadings, and special stiffness constraints have on composite panel structural efficiency.

Test results for stiffened panels designed by these improved procedures correlate well with theory when factors that affect buckling such as thickness and material property variations, initial imperfections, and transverse shear effects are adequately considered. Test results, however, also show that both low-velocity impact damage and circular holes can severely degrade the compressive strength of heavily-loaded composite panels designed to carry load at high strains. The problem is not critical for lightly-loaded designs since these panels usually carry the required load at relatively low strains. Low-velocity impact can cause local delamination and intraply cracking of the laminate. The local impact damage propagates in compression-loaded composite panels either by delamination, by local shear failure, or by a coupling between the applied axial load and the local lateral deformation due to impact. Currently, limiting the ultimate design strain based on experimental results appears to be one approach for addressing the damage tolerance problem. Although significant mass savings can still be achieved by imposing strains lower than are traditionally applied to metals, the need exists to improve the damage tolerance of composite structures. Test data indicate the impact-damage tolerance of graphite-epoxy laminates may be enhanced through improvements in the matrix material.

REFERENCES

1. Mikulas, Martin M., Jr.; Bush, Harold G.; and Rhodes, Marvin D.: Current Langley Research Center Studies on Buckling and Low-Velocity Impact of Composites Panels. Third Conference on Fibrous Composites in Flight Vehicle Design, Part II, NASA TM X-3377, 1976, pp. 633-663.

2. Wittrick, W. H.; and Williams, F. W.: Buckling and Vibration of Anisotropic or Isotropic Plate Assemblies Under Combined Loadings. Int. J. Mech. Sci., Vol. 16, 1974, pp. 209-239.

3. Almroth, B. O.; and Brogan, F. A.: The STAGS Computer Code. NASA CR-2950, February 1978.

4. Williams, Jerry G.; and Stein, Manuel: Buckling Behavior and Structural Efficiency of Open-Section Stiffened Composite Compression Panels. AIAA J., Vol. 14, No. 11, Nov. 1976, pp. 1618-1626.

5. Stein, Manuel; and Williams, Jerry G.: Buckling and Structural Efficiency of Sandwich-Blade Stiffened Composite Compression Panels. NASA TP 1269, September 1978.

6. Anon.: The NASTRAN User's Manual (Level 16.0). NASA SP-222(03), 1976.

ORIGINAL PAGE IS OF POOR QUALITY

7. Viswanathan, A. V.; and Tamekuni, M.: Elastic Buckling Analysis for Composite Stiffened Panels and Other Structures Subjected to Biaxial Inplane Loads. NASA CR-2216, September 1978.

8. Anderson, Melvin S.; and Stroud, W. Jefferson: A General Panel Sizing Computer Code and Its Application to Composite Structural Panels. A Collection of Technical Papers - AIAA/ASME 19th Structures, Structural Dynamics and Materials Conference, April 1978, pp. 14-22. AIAA Paper No. 78-467.

9. Williams, Jerry G.; and Mikulas, Martin M., Jr.: Analytical and Experimental Study of Structurally-Efficient Composite Hat-Stiffened Panels Loaded in Axial Compression. NASA TM X-72813, 1976. (Also available as AIAA Paper No. 75-754.)

10. Starnes, James H., Jr.; Rhodes, Marvin D.; and Williams, Jerry G.: The Effect of Impact Damage and Circular Holes on the Compression Strength of a Graphite-Epoxy Laminate. NASA TM 78796, October 1978.

11. Rhodes, Marvin D.; Williams, Jerry G.; and Starnes, James H., Jr.: Low-Velocity Impact Damage in Graphite-Fiber Reinforced Epoxy Laminates. Paper presented 34th Annual Conference Reinforced Plastics/Composite Institute, The Society of the Plastics Industry, Inc. New Orleans, Louisiana, January 29 - February 2, 1979.

12. Rhodes, Marvin D.; Williams, Jerry G.; and Starnes, James H., Jr.: Effect of Low-Velocity Impact Damage on the Compressive Strength of Graphite-Epoxy Hat-Stiffened Panels. NASA TN D-8411, 1977.

13. Rhodes, Marvin D.; Williams, Jerry G.; and Starnes, James H, Jr.: Effect of Impact Damage on the Compression Strength of Filamentary-Composite Hat-Stiffened Panels. Selective Applications of Materials for Products and Energy. Vol. 23 of National SAMPE Symposium and Exhibition, Society of Advanced Material and Process Engineering, May 1978, pp. 300-319.

14. Anon.: A Study on the Utilization of Advanced Composites in Commercial Aircraft Wing Structure. NASA CR-158902-2, 1978.

ORIGINAL PAGE IS
OF POOR QUALITY